# EFFECT OF TRANSPORT VARIABLES ON ACID JETTING IN CARBONATES

A Thesis

by

DMITRY RIDNER

Submitted to the Office of Graduate and Professional Studies of Texas A&M University
in partial fulfillment of the requirements for the degree of

MASTER OF SCIENCE

| | |
|---|---|
| Chair of Committee, | Ding Zhu |
| Committee Members, | A. Daniel Hill |
| | Yuefeng Sun |
| Head of Department, | Jeff Spath |

August 2018

Major Subject: Petroleum Engineering

## ABSTRACT

Acid jetting is a well stimulation method that occurs in limited entry liner completions. Fluid exiting on orifice experiences a significant pressure drop as a high velocity stream impinges against the wellbore wall. Two types of dissolution patterns occur in the process: a cavity formed by surface dissolution and wormholes formed beyond the cavity as a result of a pressure drop between the wellbore and the reservoir. Jetting has been previously used to place acid in horizontal wells, as well as for wellbore cleanup, filter cake removal and stimulation enhancement. These dissolution mechanisms depend on transport variables such as acid injection rate, velocity of the jet, temperature, and permeability of the formation. Jetting changes these variables and as a result the variation in stimulation result between the matrix dissolution mechanism of acid jetting and that of conventional matrix acidizing is most significant at lower interstitial velocities. This study involves the experimental investigation of the comparative wormhole growth of acid jetting versus matrix acidizing, as well as a study of the effect of the abovementioned variables including increased temperature, rock permeability and acid concentration on the efficiency with respect to acid injection rate. The experiments were conducted with a controlled case of 15% HCl and 2-4 mD Indiana limestone and subsequently compared with experiments conducted at 180°F and 28% HCl. The influence of jetting velocity on the jetting outcome was examined by altering the output of the acid injection pump. The results of the experiments were then examined alongside non-jetting cases, which was run in core floods that eliminated the jetting effect of the stream by way of mechanical dispersion. Acid jetting creates a pressure spike point at the face of the wellbore, leading to a heightened interstitial velocity at the contact of the acid and the rock. This results in wormhole propagation occurring at a faster rate than it would in conventional matrix acidizing at an equivalent rate of

injection. This phenomena is particularly significant as jetting velocity is increased beyond that of matrix acidizing, and becomes progressively less dramatic at higher jetting velocities. The findings from this study helps to develop the understanding of the mechanism of acid jetting and optimize jetting design.

## DEDICATION

I dedicate this work to my loving parents, Vitaly and Tatiana, as well as my wonderful sister, Michal.

## ACKNOWLEDGEMENTS

I would like to thank my committee chair, Dr. Ding Zhu for supporting and guiding me in my master's degree at Texas A&M University, as well as giving me an opportunity to work on this project. It has been an incredible learning experience for me and I greatly appreciate the professional and personal growth it has given me. I would also like to thank Dr. Dan Hill and Dr. Yuefeng Sun for their contributions and recommendations throughout my work.

The experiments described in this project would not be possible without the tireless help of my project partners, Taylor Frick and Vanessa Ndonhong. I'm extremely grateful to have had the chance to work with them on this study.

## CONTRIBUTORS AND FUNDING SOURCES

### Contributors

This work was supported by a thesis committee consisting of Professor Ding Zhu and Professor A. Daniel Hill of the Department of Petroleum Engineering and Professor Yuefeng Sun of the Department of Geology and Geophysics.

The experiments whose data is included in this study were conducted jointly by Dmitry Ridner and Taylor Frick of the Department of Petroleum Engineering.

### Funding Sources

This study was supported by funding from the ExxonMobil Upstream Research Company.

## NOMENCLATURE

| | |
|---|---|
| $A$ | Cross-sectional area of the core |
| $A_{nozzle}$ | Cross-sectional area of the nozzle |
| CT | Computed Tomography |
| $D_{core}$ | Diameter of the core |
| DICOM | Digital Imaging and Communications in Medicine |
| $D_{nozzle}$ | Inner diameter of the nozzle |
| HCl | Hydrochloric acid |
| $k$ | Permeability |
| $L$ | Length of the core |
| $m_{dry}$ | Dry mass |
| $m_{sat}$ | Saturated mass |
| $n$ | Number of stages |
| $q$ | Flow rate through the core |
| $q_{effluent}$ | Effluent flow rate |
| $q_{max}$ | Maximum pump flow rate |
| $q_{pump}$ | Pump flow rate |
| $v_{cav}$ | Cavity growth rate |
| $v_{wh}$ | Wormhole growth rate |
| $V_{bulk}$ | Bulk volume |
| $v_i$ | Interstitial velocity |
| $v_{jet}$ | Jetting velocity |

| | |
|---|---|
| $V_{pore}$ | Pore volume |
| $\Delta P$ | Pressure differential |
| $t_{jet}$ | Jetting time |
| $\mu$ | Viscosity |
| $\rho_w$ | Density of water |
| $\phi$ | Porosity |

## TABLE OF CONTENTS

Page

## LIST OF FIGURES

Page

# 1. INTRODUCTION

Acid stimulation of extended reach wells in carbonate reservoirs through the use of limited entry liners has been well documented before (Hansen and Nederveen, 2002). The process involves the injection of acid through a centralized, non-cemented liner in the wellbore, through which it exits via several orifices at high velocity. This results in a jetting effect as the acid impinges onto the face of the rock in the annular space between the liner and the open hole (Beckham, 2015). Jetting was initially applied in the industry for the purpose of borehole cleaning (Suraatmadja, 1994) and localized filter cake removal (Johnson, 1998).

Developments in the drilling of horizontal, extended-reach wells present new challenges in effective acid stimulation of the lateral. Long laterals pass through a wide range of heterogeneities in lithology, including natural fractures. Due to this, the need for controlled acid placement and diversion becomes highly important. Simply bullheading acid into the well with no means of diversion results in overstimulation of the heel of the well, leaving the lateral closer to the toe understimulated. Acid diversion can be achieved through both mechanical and chemical means (Glasbergen, 2006). Acid jetting can be used as a mechanical acid placement technique by way of predetermined location points of acid entry. This was initially achieved through the use of coiled tubing or drill pipe. Drill pipes have a set of nozzles at the end of the string and are gradually moved along the lateral during injection, as shown in Figure 1.1 and Figure 1.2. However, these methods are less effective in extended-reach wells due to the limitations in their reliability and economics.

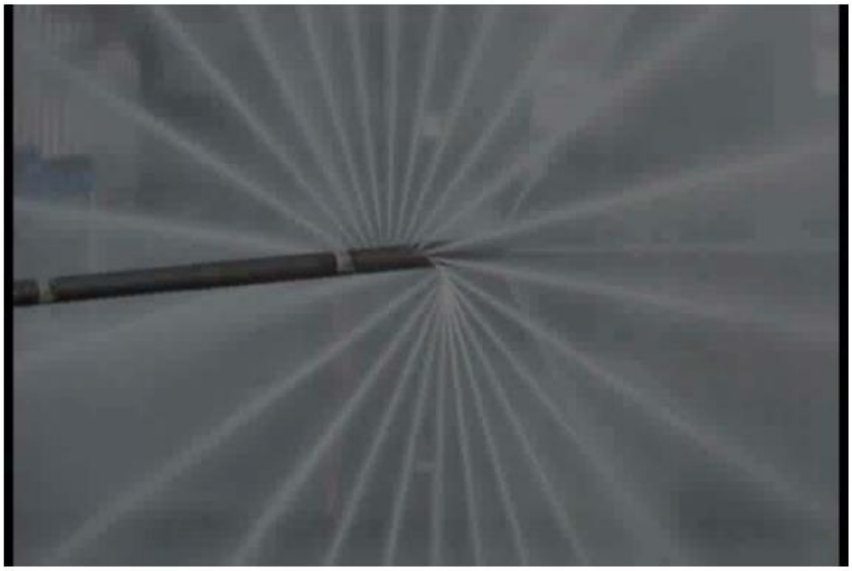

**Figure 1.1 - Spiral jet tool on drill pipe (Jorden et al. 2011)**

**Figure 1.2 - Close-up of drill pipe jetting tool (Ritchie, 2008)**

Limited entry liners (LEL) with zonal isolation packers have been used to successfully distribute acid uniformly in the lower completion with strategically placed

orifices for the acid to exit. Figure 1.3 shows the flow pattern in such a liner downhole. This gives limited entry liners the advantage of tuning the pressure drop along the liner length, with more orifices present at the toe of the liner and fewer at the heel of the liner. Limited entry liner completions have been used to stimulate 11,200 ft lateral lengths with 28% HCl with a 12 compartment liner (Jorden, 2012). Distribution of the orifices resulted in a 177 ft/s jetting velocity at a 25 bbl/min injection rate, and PLT analysis indicated that the entire lateral had been stimulated (Jackson, 2012). The design of such completion for implementation of acid jetting in limited entry liners requires a more thorough understanding of the dissolution process and its optimal operating conditions.

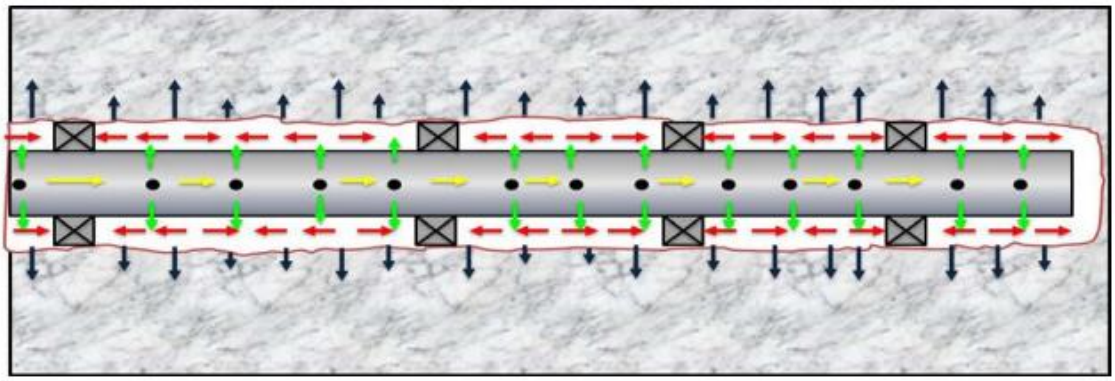

**Figure 1.3 - Flow in limited entry liner (LEL) completion**

Acid jetting is similar to matrix acidizing in that it not only allows for wellbore cleanup and filter cake removal, but also results in a reduction of wellbore skin through wormholing. Matrix acidizing has been well-documented in the industry for many decades, and there is a firm understanding of its behavior through extensive laboratory (Fredd, 1999) and field experiments (Furui, 2010), as well as analytical (Hoefner, 1989; Hung, 1989; Buijse, 2005; Furui, 2010) and numerical modelling (Schwalbert, 2017). The

dissolution structure formed through jetting however, is influenced by a larger set of transport variables in addition to the flux of the acid injection, and these effects still need to be quantified. A notable difference between the two phenomena include the formation of a cavity due to the impingement of the jet on the rock face.

The jetting effect observed in the field has previously been studied on a laboratory scale through linear core flood experiments (Ndonhong, 2017). The acidizing process results in the formation of two distinct dissolution structures. A cavity is formed around the impingement location of the jet on the rock face, and wormholes propagate through the rock beyond the cavity. Figure 1.4 shows the photos of the outside of such a core flood experiment and Figure 1.5 shows a computer tomography (CT) scan of the dissolution structures inside. These experiments are similar to those conducted for the study of matrix acidizing, but differ in the flow pattern of the acid through the core holder. In matrix acidizing, there is only one outlet for the acid and thus all of the injected acid flows through the rock. In acid jetting on the other hand, the inclusion of a narrow nozzle through which the acid travels into the core holder creates a situation where the rate of injected acid is higher than the rate that flows through the core. This creates a need for a relief or return line for the remaining volume of acid to evacuate. This results in a more complex flow pattern that is challenging to describe and model within the framework of industry-established matrix acidizing analysis.

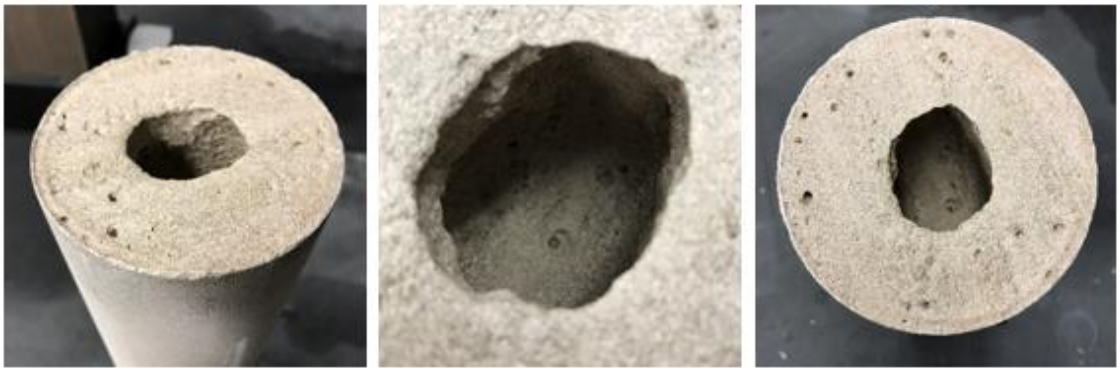

**Figure 1.4 - Exterior of 4" limestone core after lab scale acid jetting**

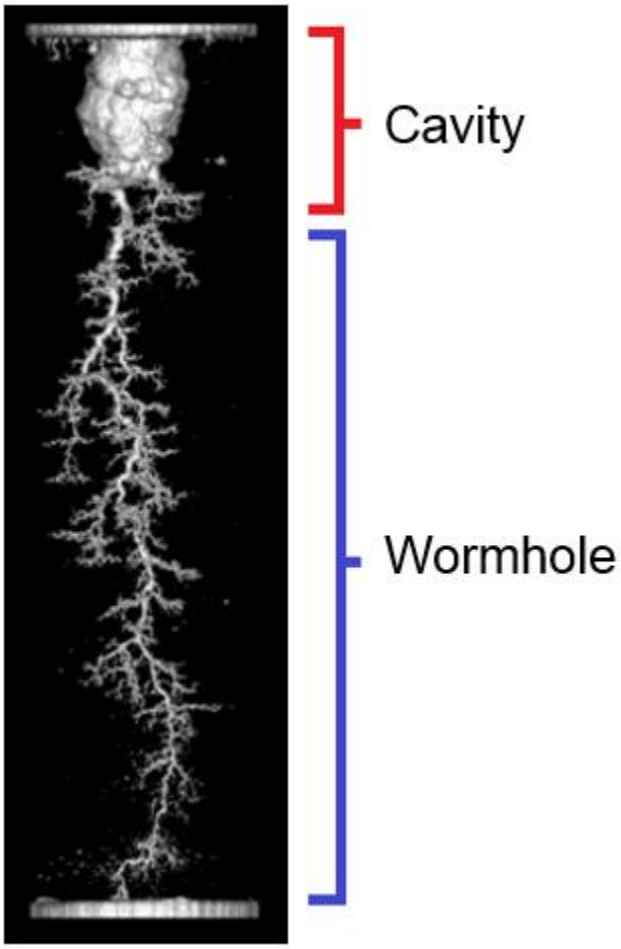


**Figure 1.5 - CT image of acid jetting dissolution structure**

Previous experimental studies conducted by Holland (2014), Ndonhong (2014) and Belostrino (2016) on acid jetting at jetting velocities of 100 ft/s and 200 ft/s have shown that the cavity and wormholing occur simultaneously during the injection process. Studies on acid jetting in differing rock type have indicated that pore structure also influence dissolution outcome. Overall, it has been observed that cavity growth rate is influenced by jetting velocity, while the dominant variable in wormhole propagation is acid flux, or interstitial velocity. The particular effect that jetting has on matrix dissolution must still be quantified in a way that is directly comparable with conventional matrix acidizing.

This study aims to provide an objective means of comparison between the two phenomena, as well as characterize the effect of transport conditions such as temperature, jetting velocity, and acid concentration on the outcome of the dissolution in acid jetting.

# 2. EXPERIMENTAL APPARATUS

## 2.1 Overall Setup

The experimental apparatus used for this study is the same as the one used by Holland (2014), Ndonhong (2014) and Belostrino (2016), with the addition of a flow control valve downstream of the core holder, and a weight scale with a collection beaker at the end of the effluent line. The modifications to the setup are described in the following section. Figure 2.1 provides a schematic of the updated experimental apparatus.

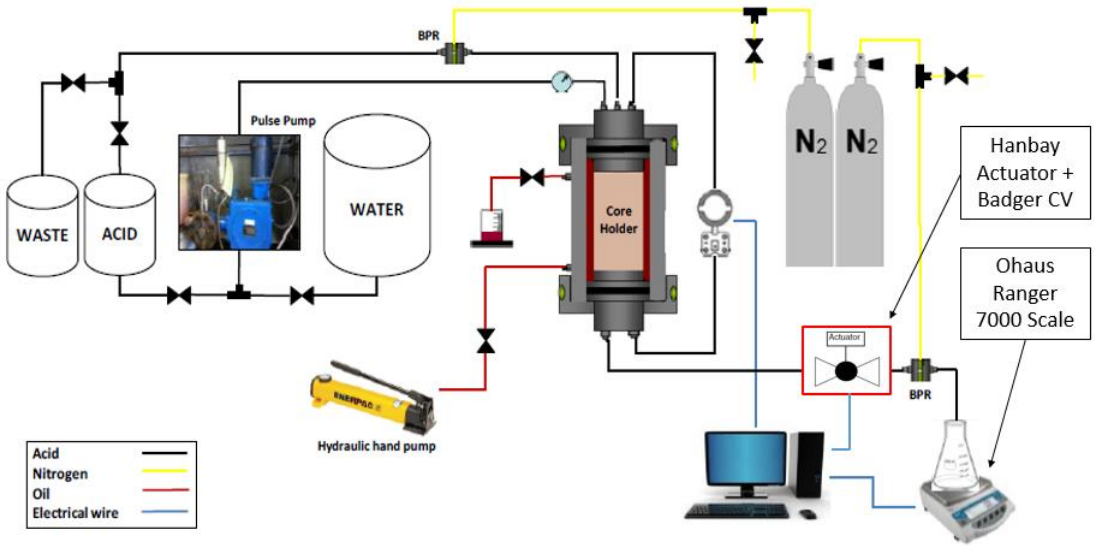


**Figure 2.1 - Acid Jetting Experimental Setup Schematic (Reprinted from Holland, 2014)**

The experimental apparatus uses a Chem/Meter 800 series pulse pump to transport acid to a hassler type core holder that can hold 4" diameter core samples. Figure 2.2 shows a schematic of the core holder and its surrounding lines.

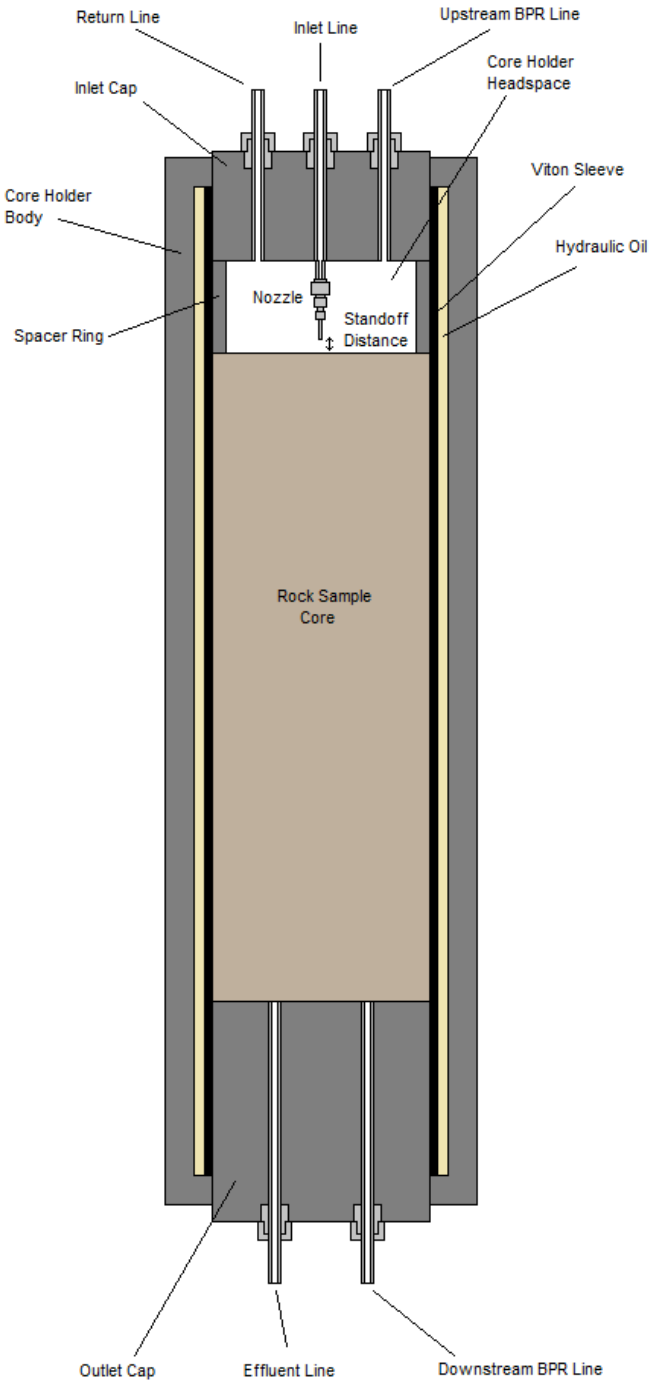


**Figure 2.2 - Acid Jetting Core Holder Schematic**

The inlet cap contains an inlet line through which the acid enters the headspace of the core holder. The acid that does not flow through the rock sample is subsequently transported through the return line on the inlet cap to a waste container. The pressure on the upstream side of the rock sample is maintained constant by way of the upstream back pressure regulator (BPR) line on the inlet cap.

The acid that does flow through the rock sample exits the core holder through the effluent line on the outlet cap downstream of the rock sample. The pressure on this side is maintained by way of the downstream back pressure regulator line on the outlet cap. Both of the back pressure regulators on the core holder are connected to separate compressed nitrogen tanks, which supply the gas to maintain the pressure. The pressure differential between the two sides of the core results in a flow rate through the core, whose rate is dependent on the permeability of the rock (Darcy's Law). This flow rate is normalized for different core diameters and rock permeability by conversion to a flow per area, otherwise known as interstitial velocity. Calculations for these flow rates are described in details in the Experimental Procedure section.

An Enerpac Co. Model P392 hand pump is used to pump hydraulic oil into a Viton sleeve situated within the holder. This is used in order to increase the confining pressure around the rock sample, such that it is maintained above the pressure set on the upstream of the core. This is done in order to prevent any flow along the side of the core, and thereby ensuring that all flow travels through the rock pores and resulting in a correct interstitial velocity.

## 2.2 Modifications to Setup

### *2.2.1 Effluent Line Weight Scale*

In order to determine the flow rate of the effluent line from the core, an OHAUS Ranger 7000 scale was installed at the end of the line. The scale was connected to the computer through a USB cable, allowing it to transmit readings to the LabVIEW program every 0.5 sec during experiments as a steady stream of data. Figure 2.3 displays the scale setup and the container used to collect the effluent volume.

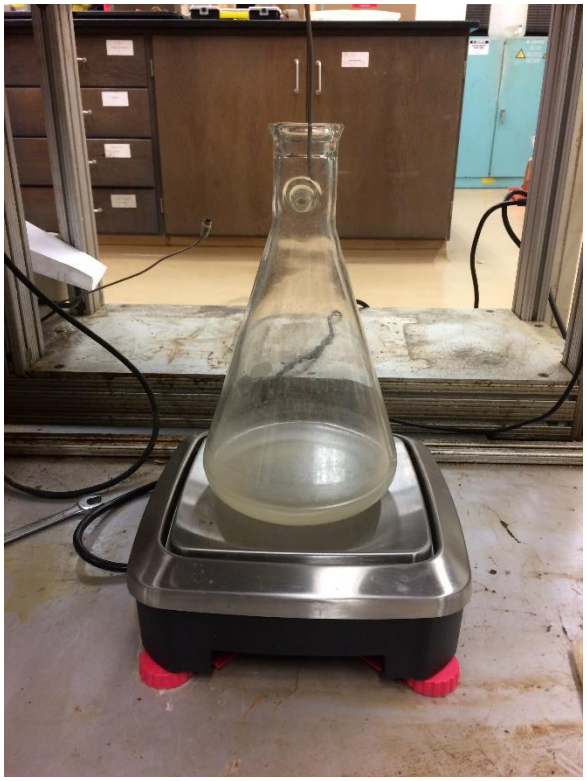

**Figure 2.3- OHAUS Ranger 7000 Scale (pictured with Erlenmeyer flask)**

In order to obtain a flow rate from the mass scale, an assumption was made that the density of the effluent was approximately the same as that of water (1 g/mL). The mass readings from the scale were converted to a flow rate in LabVIEW the following way:

$$\bar{m} = \frac{1}{n}\sum_{i=0}^{n-1} m_i \tag{1}$$

$$\frac{\Delta\bar{m}}{\Delta t} = \frac{\bar{m}_i - \bar{m}_{i-1}}{\Delta t} \tag{2}$$

Where $m_i$ is the individual data point of mass is collected by the scale (measured in g), $n$ is the number of data points, and $\bar{m}$ is the average mass. This allows for the change in mass to be calculated as a moving average over an interval of points (50 points were used in this case), and then subtracted over the interval of time between recordings ($\Delta t$, measured in s seconds) in Equation 2. This moving average allows for a smoothening of the rate of change and removal of fluctuations due to noise. The resulting rate of mass change in g/s is equivalent to the effluent flow rate in mL/s under the density assumption. The flow rate is converted to interstitial velocity ($v_i$) by way of:

$$q_{effluent} = \frac{\Delta\bar{m}}{\Delta t}\rho_{effluent} = v_i A\phi \tag{3}$$

Where $\rho_{effluent}$ refers to the density of the effluent stream, which contains water and spent acid, $A$ is the cross-sectional area of the core, and $\phi$ is the porosity of the rock. The limitation of this calculation method is that the large number of data points needed to smooth the rate of change in the moving average calculation induces a lag time between when the change occurs in the core and when the change is observed in the data. This can become a problem during core breakthrough, when the effluent flow rate rises exponentially and requires an immediate shutoff of the system.

### *2.2.2 Effluent Line Flow Control Valve and PID Controller*

For the purpose of this study, it was desired to keep the interstitial velocity constant throughout the jetting time of each experiment. In acid jetting experiments conducted previously by Holland (2014), Ndonhong (2014) and Belostrino (2016), interstitial velocity was not controlled throughout the course of the experiment, and it was observed that the interstitial velocity steadily increased from the start of the jetting time, culminating in an exponential rise near breakthrough. In order to prevent this change in flow, a flow control valve was installed on the effluent line from the core holder, shown in Figure 2.4.


**Figure 2.4 - Hanbay actuator and Badger flow control valve**

The flow control valve setup consisted of two components: An LCx-xxxAx-8.06 Actuator manufactured by Hanbay Inc., along with a high pressure hastelloy needle valve

from Badger Inc. The flow coefficient of the valve ($C_v$) was 0.0004, and the clearance of the needle ($D_v$) was 0.25 in.

The actuator was linked to the LabVIEW program by way of a Turck-6 cable connected from the outlet on the actuator body to the NI board of the computer. The actuator functioned as a communication instrument between the settings made on the LabVIEW and the movement of the needle valve. The control of the flow through the valve on the LabVIEW program was performed by way of a PID (proportional, integral, derivative) feedback control loop.

A closed PID feedback control loop continuously determines the difference between the measured variable (in this case, the flow rate though the effluent line) and the desired set point of that variable. A subsequent correction is applied based on a proportional gain, integral time and derivative time value. This correction takes the form of the movement of the valve. Figure 2.5 describes this feedback control loop. In the context of this experimental setup, the system refers to the effluent from the core holder, while the sensor refers to the reading on the weight scale that collects the effluent at the end of the line.

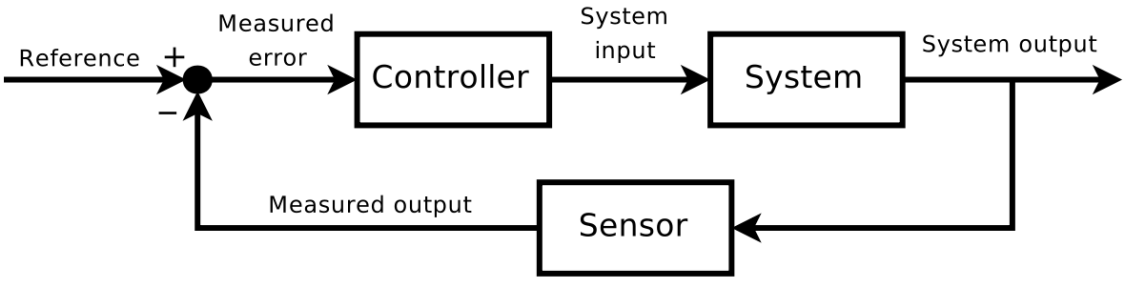


**Figure 2.5 - Closed Loop Control Schematic**

A commonly used heuristic method for calculating these PID values is the Ziegler-Nichols tuning method in an open loop test. An open loop differs from a closed one in that the controller input to the system is made manually, and there is no feedback of the measured variable output to the controller. Figure 2.6 portrays an open loop test.

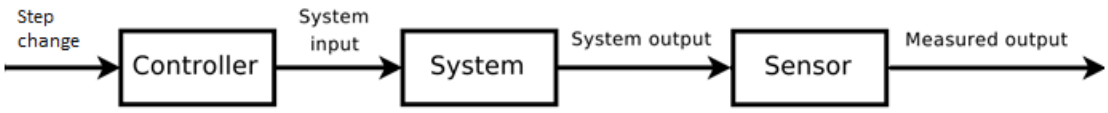


**Figure 2.6 - Open Loop Control Schematic**

A Ziegler-Nichols open loop test is conducted in the following way:

1. Allow system to reach steady state
2. Make a step change in the controller output and wait until the process variable (in this case the effluent output) reaches steady state again.
3. Calculate the process gain ($g_p$): the percent change in the process variable over the percent change of the controller output in the induced step change. This value is dimensionless.

$$g_p = \frac{\%\ change\ in\ process\ variable\ output}{\%\ change\ in\ controller\ output} \quad (4)$$

4. Find the inflection point, or maximum slope in the change of the process variable. The tangent of this slope and the intersection of the original process variable output marks the beginning of the response time.
5. Calculate the dead time ($t_d$): the time between the step change and the beginning of the response time, measured in seconds.

$$t_d = t_{response\ start} - t_{step\ change} \quad (5)$$

6. Calculate the time constant ($\tau$): the time it takes to reach 63% of the new process variable output after the beginning of the response time, measured in seconds.

$$\tau = t_{63\%\ of\ total\ change} - t_{response\ start} \quad (6)$$

7. For PID control, the controller gain ($K_c$), the integral time ($T_i$) and derivative time ($T_d$) are calculated as:

$$K_c = \frac{1.2\tau}{g_p t_d} \quad (7)$$

$$T_i = 2t_d \quad (8)$$

$$T_d = 0.5t_d \quad (9)$$

The units for $T_i$ and $T_d$ are seconds, while $K_c$ is dimensionless. These PID values are used to calculate the correction needed to be made to the system iteratively in order to bring the measured variable to the desired set point. The relationship between the deviation or error from the set point and the needed response is calculated in the Laplace domain:

$$G_{PID}(s) = \frac{U(s)}{E(s)} = K_c\left(1 + \frac{1}{T_i s} + T_d s\right) \quad (10)$$

Where $U(s)$ is the correction made by the controller as a function of Laplace time ($s$), and $E(s)$ is the error from the set point as a function of Laplace time. This equation is built into the LabVIEW program, so the only parameters that need to be specified by the user are the gains $K_c$, $T_i$ and $T_d$ obtained when the open loop test is conducted. If there is no deviation from the set point, the controller does not act. Although the Ziegler-Nichols

tuning method provides reliable estimates of the PID controller gains, some manual fine-tuning is usually required to obtain an optimum response behavior from the controller.

# 3. EXPERIMENTAL PROCEDURE

This study involved the use of limestone cores acidized by way of acid jetting in a linear core flood apparatus. This section describes core preparation, calculation of rock characteristics, the experimental apparatus, experimental procedure, as well as how experimental results were analyzed.

## 3.1 Core Description and Preparation

The cores used in this study consisted of Indiana limestone, along with field cores composed of a dolomitic limestone and calcareous dolomite. The cores were all 4" in diameter, with variable lengths of 16" and 8". The Indiana cores were supplied by Kocurek Industries and the field cores were supplied by the sponsoring company. All cores were identified with a unique, two-letter and two-number label. Although approximate rock properties for the cores were given by the suppliers in advance, their exact values required verification. Figure 3.1 displays the visual appearance of one of the cores.

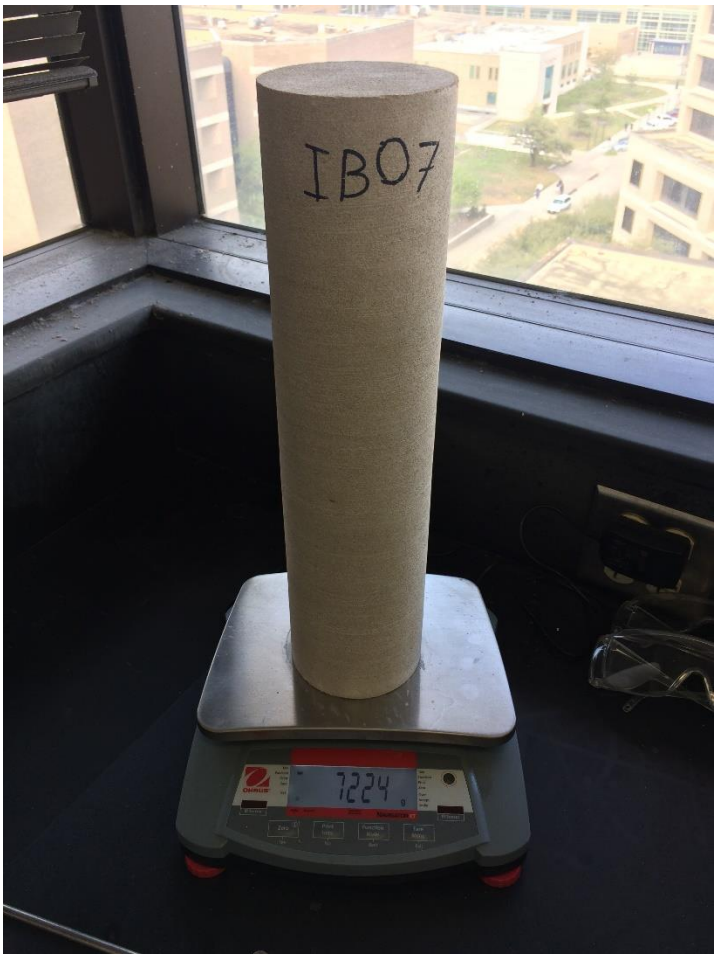


**Figure 3.1 - Unsaturated Indiana limestone core exterior prior to acidizing**

### *3.1.1 Porosity Calculation via Core Saturation in Water*

In order to determine the porosity of the rock for each sample, each core was saturated with water and the difference in weight was recorded. The dry cores were initially weighed to record the mass of the rock in air. Each core was subsequently places in a cylindrical water-filled container, as shown in Figure 3.2. The water level in the container was maintained such that the core would not be exposed to air when water would completely fill its pores after the saturation process.

**Figure 3.2 - Saturation container and vacuum pump setup**

A Leybold Trivac Model D2A vacuum pump was used to assist the saturation process. The vacuum pump decreased the pressure above the surface of the water in the container holding the core, allowing the air to be displaced faster, and more easily flow out of the rock pores. A tight seal on the cap of the core container was necessary to

maintain the vacuum in system. As with previous studies conducted by Holland (2014), Ndonhong (2014) and Belostrino (2016), each core was allowed at least 8 hours to saturate.

After saturation, the wet weight of each core was recorded. Porosity was calculated in the following way:

$$\phi_{core} = \frac{(m_{wet} - m_{dry})}{\rho_{water} V_{core}} = \frac{(m_{wet} - m_{dry})}{\frac{1}{4}\pi \rho_{water} d_{core}^2 L_{core}} \quad (11)$$

Where $\phi_{core}$ is the porosity of the core (expressed as %), $\rho_{water}$ is the density of water (measured in g/in$^3$), $L_{core}$ is the length of the core (measured in inches), $L_{core}$ is the diameter of the core (measured in inches), while $m_{dry}$ and $m_{wet}$ are the dry and saturated mass of the core respectively (measured in g). This equation uses the density of water to convert difference in mass due to water saturation into volume occupied by pore space.

### *3.1.2 Permeability Calculation via Darcy's Law*

The permeability measurement apparatus used for this study is identical to that which is described by Grabski (2012) and subsequently used by Holland (2014), Ndonhong (2014) and Belostrino (2016). The procedure involves flowing water through each core at a constant flow rate and recording the resulting pressure differential. The core holder used for this setup has the same dimensions as that which is used for the acid jetting experimental setup in this study. As seen in Figure 3.3, the setup consists of a core holder (only the first one of the two depicted in the schematic is used) with a pressure transducer connected to the upstream and downstream lines. Water is pumped from a water

accumulator to the core holder by way of a syringe pump, which alters flowing pressure to ensure a constant flow rate.

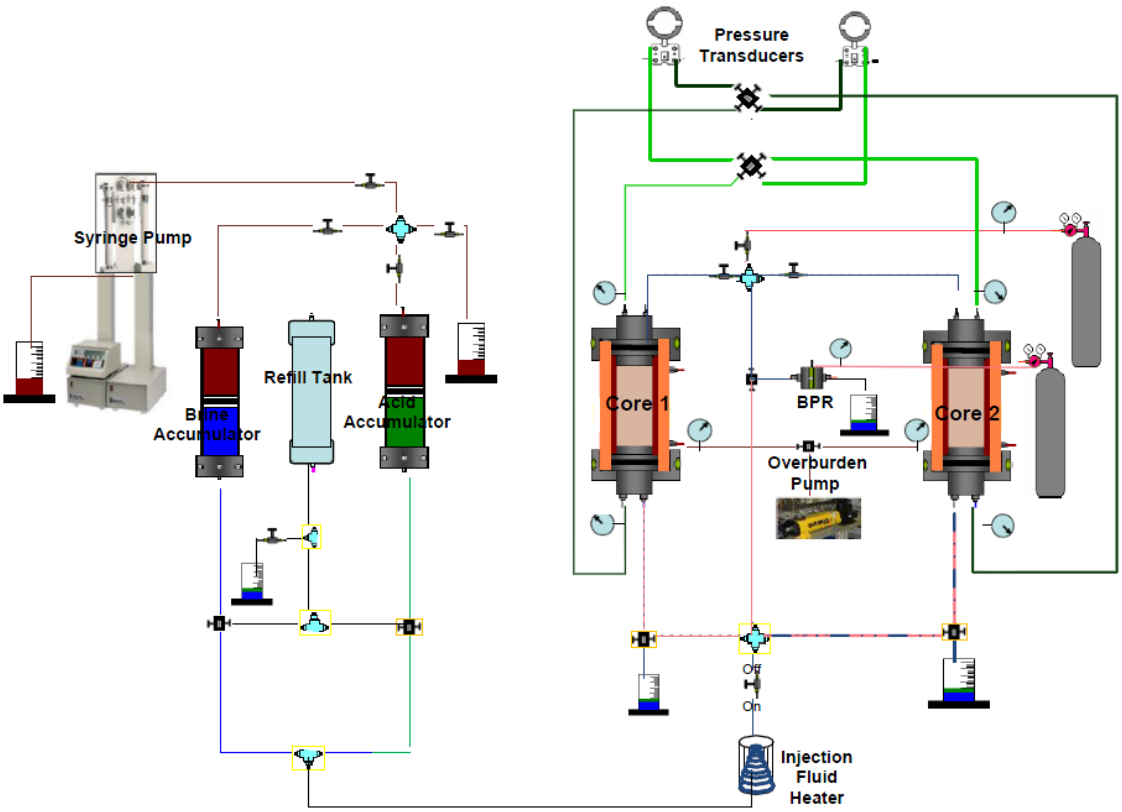


**Figure 3.3 - Permeability Test Experimental Setup (Reprinted from Grabski, 2012)**

The pressure transducer relays pressure data to a LabVIEW program on a computer. When the flow of water through the core and corresponding pressure differential reaches steady state, the permeability of the core can be determined by way of Darcy's Law:

$$k = \frac{96.13 q L_{core} \mu_{water}}{\Delta P A_{core}} \tag{12}$$

The conversion factor in this form of Darcy's Law requires units of flow rate ($q$) in mL/min, core length ($L_{core}$) in inches, water viscosity ($\mu_{water}$) in centipoise, pressure differential ($\Delta P$) in psi and the area of the core face ($A_{core}$) to be in square inches, resulting in a permeability value ($k$) in units of mD.

## 3.2 Acid Jetting Procedure

The experimental procedure in this study is based on the one described by Holland (2014), with several modifications. The procedure includes preparation of acid, pump adjustment and verification, water flush, acid injection and a final water flush.

### *3.2.1 Acid Preparation*

The acid used in this study is hydrochloric acid (HCl). It is purchased as a stock solution from Macron Chemical Company, having a weight by weight concentration of 38.5%. The baseline concentration used for the experiments in this study is 15%. In order to achieve this concentration, the following ratio of water to stock solution is used:

$$V_{stock} = 0.356V_{total} \quad V_{water} = 0.644V_{total} \tag{13}$$

Where $V_{total}$ is the total volume of solution used in the experiment, $V_{stock}$ is the volume of stock solution required, and $V_{water}$ is the volume of water needed to be added to achieve the desired acid concentration, with all volumes measured in L. In experiments run at 28% concentration, the stock solution volume is increased:

$$V_{stock} = 0.712V_{total} \quad V_{water} = 0.288V_{total} \tag{14}$$

In all experiments, 5 mL of corrosion inhibitor (Schlumberger A262) is used for every 1000 mL of acid solution.

### *3.2.2 Pump Adjustment for Constant Flow*

In experiments performed by Holland (2014), Ndonhong (2014) and Belostrino (2016), the pump injection rate was set prior to the start of every experiment to achieve the desired jetting velocity. The pump setting was adjusted accordingly to ensure the same flow rate when the pump is started. This type of procedure was also performed for experiments performed on 4" by 16" Indiana limestone cores in this study (22 in total). The relationship between pump setting and jetting velocity is:

$$q_{pump} = q_{max}(capacity\%) = \left(16.3\frac{gal}{hr}\right)(capacity\ \%) \tag{15}$$

$$q_{pump} = \left(16.3\frac{gal}{hr}\right)\left(0.133681\frac{ft^3}{gal}\right)\left(\frac{1\ hr}{3660\ s}\right)(capacity\ \%) \tag{16}$$

$$q_{pump} = \left(5.9535\ \cdot 10^{-4}\frac{ft^3}{s}\right)(capacity\ \%) \tag{17}$$

$$A_{nozzle} = \frac{\pi}{4}D_{nozzle}^2 = \frac{\pi}{4}\left[(0.0225\ in)\left(\frac{1\ ft}{12\ in}\right)\right]^2 = 2.7612\ \cdot 10^{-6}\ ft^2 \tag{18}$$

$$v_{jet} = \frac{q_{pump}}{A_{nozzle}} = \frac{\left(5.9535\ \cdot 10^{-4}\frac{ft^3}{s}\right)(capacity\ \%)}{2.7612\ \cdot 10^{-6}\ ft^2} = \left(215.613\frac{ft}{s}\right)(capacity\ \%) \tag{19}$$

The flow rate ($q_{pump}$) from the pump is measured in gal/hr. The maximum flow rate ($q_{max}$) of the pump is 16.3 gal/hr, and the capacity % refers to the fraction of the maximum flow rate that the pump is running at, which can be adjusted on by a knob on

the pump, as shown in Figure 3.5. The subsequent jetting velocity from the nozzle ($v_{jet}$) is expressed as a ratio of the pump flow rate and the cross sectional area of the nozzle ($A_{nozzle}$), calculated from the diameter of the nozzle ($D_{nozzle}$).

It was determined that setting the pump to the same setting and rate at the start of flow, however, does not yield the same injection flow rate at differing interstitial velocities. This is due to the pump output being affected by the upstream backpressure induced in the headspace of the core holder. According to the pump manual, pump output will decrease by approximately 1.5% for every 100 psi increase in pressure. In this setup, however, there is a minimum backpressure on the upstream of 1000 psi, with additional pressure added as interstitial velocity is required to be increased. Since the pump limit is 1900 psi, at high upstream back pressure the strokes of the pump approach this limit and there is a significant decrease in flow rate.

The pump was tested for this behavior at three different pump settings featured in the work of Holland (2014): 48.75%, 68.5% and 91.5%. According to the above relations, these pump settings are supposed to result in jetting velocities of 107 ft/s, 150 ft/s and 200 ft/s respectively. However, when progressively higher upstream backpressure is induced on the inlet line and core holder headspace, a progressively lower flow rate (and therefore jetting velocity) is observed. Figure 3.4 shows these trends for the three pump settings.

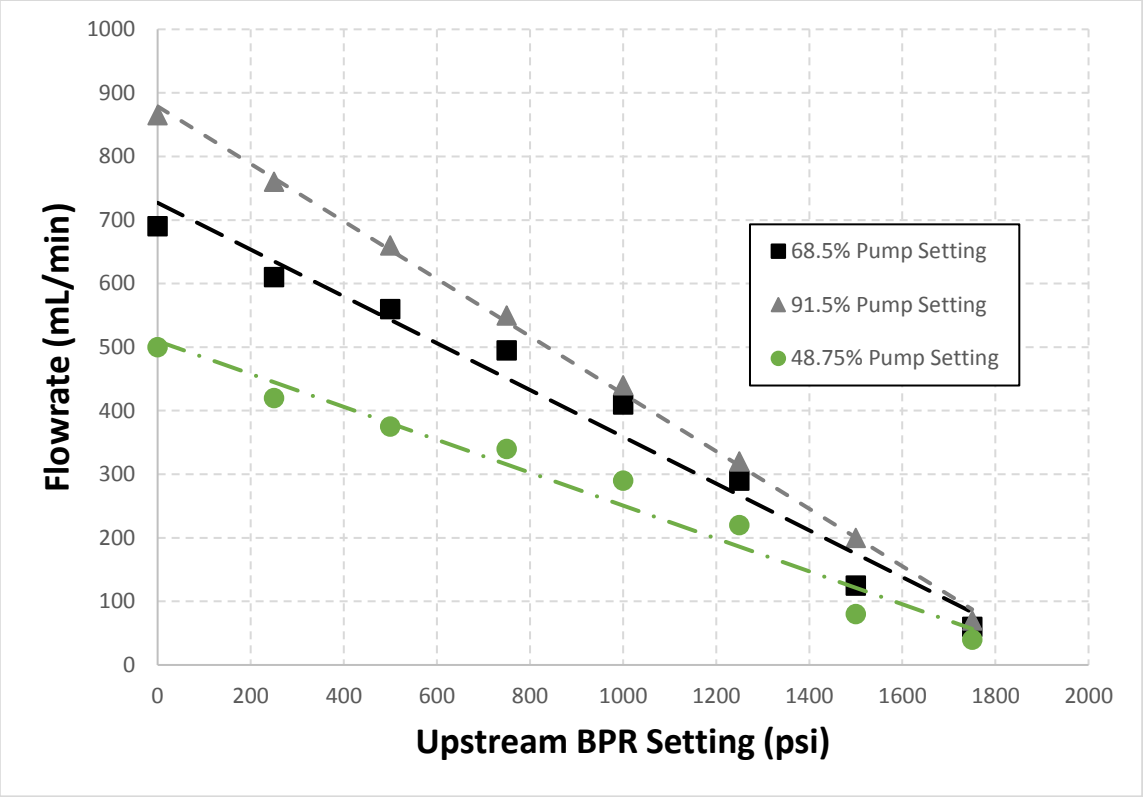


**Figure 3.4 - Pump flow rate change as a function of upstream backpressure at varying pump setting percentages**

The flow rate shown in the plot was measured at the end of the return line. The flow was collected in a graduated cylinder and a stopwatch was used to measure an interval of one minute. It can be observed from the plot that there is a negatively proportional relationship between pump output and upstream back pressure, and that for all tested pump settings, the flow rates converge to zero when the upstream backpressure approaches the pump limit of 1900 psi.

The general relationship of the pump output with respect to upstream backpressure can be described as:

$$q_{pump} = -\frac{q_{atm}}{P_{max}} p_{upstream\,BPR} + q_{atm} \quad where \;\; P_{max} = 1950\,psi \tag{20}$$

In this relationship, $q_{pump}$ is the pump flow rate, $p_{upstream\,BPR}$ is the upstream backpressure, and $q_{atm}$ refers to the flow rate when no upstream backpressure is applied, and $P_{max}$ is the maximum pressure the pump can handle. $q_{atm}$ is the flow rate that was tested and used in previous studies to estimate jetting velocity.

In order to determine the pump setting needed to obtain a desired jetting velocity (in ft/s) given an upstream backpressure setting (in psi), the following relationship can be used:

$$q_{pump} = v_{jet} A_{nozzle} = v_{jet}(2.7162 \cdot 10^{-6} ft^2)\left(\frac{1.699 \cdot 10^6\, mL/min}{1\frac{ft^3}{s}}\right) \tag{21}$$

$$q_{pump} = \left(4.683\ \frac{mL\ s}{ft\ min}\right) v_{jet} \tag{22}$$

When no upstream backpressure is applied:

$$q_{atm} = \left(5.9535\ \cdot 10^{-4}\frac{ft^3}{s}\right)(capacity\ \%) = \left(1028.4\frac{mL}{min}\right)(capacity\ \%) \tag{23}$$

Combining the relations gives:

$$q_{pump} = \left(\left(1028.4\frac{mL}{min}\right)(capacity\ \%)\right)\left(1 - \frac{p_{upstream}}{1950\ psi}\right) = \left(4.683\ \frac{mL\ s}{ft\ min}\right) v_{jet} \tag{24}$$

$$capacity\ \% = \frac{\left(4.683\ \frac{mL\ s}{ft\ min}\right) v_{jet}}{\left(1028.4\frac{mL}{min}\right)\left(1 - \frac{p_{upstream}}{1950\ psi}\right)} \tag{25}$$

$$capacity\ \% = 0.004554\frac{v_{jet}}{\left(1 - \frac{p_{upstream}}{1950}\right)} \tag{26}$$

With this equation, for any upstream back pressure (in psi) and desired jetting velocity (in ft/s), an appropriate pump setting can be determined. In practice however, the pump setting requires slight trial and error manipulation to obtain a consistent flow rate at differing upstream back pressures.

### *3.2.3 Baseline Experimental Procedure*

The general acid jetting procedure used in this study can be found in detail in the work by Holland (2014). Firstly the saturated core is placed inside the core holder from one end. The spacer rings are then inserted from the inlet side of the core holder, followed by the inlet cap. The core and spacers are pushed against the inlet cap to ensure that their surfaces are flush with one another. The outlet cap is then inserted after the core, closing off the end of the core holder. The outlet cap is secured in place by a screw-in fastener lock. The assembled core holder can be seen in Figure 3.5, oriented vertically with the inlet of the core holder on top and outlet on the bottom.


**Figure 3.5 - Acid Jetting Experimental Setup**

The inlet line from the pulse pump to the inlet cap, the return line from the inlet, and the hydraulic oil lines are connected to the core holder. The hydraulic oil lines supply oil to the Viton sleeve in the core holder to regulate confining pressure around the core. The lines into and out of the Viton sleeve are initially opened and hydraulic oil is pumped through the lines until a steady, uninterrupted stream exits the sleeve, indicating the removal of trapped air in the sleeve. The exit from the sleeve is then closed and hydraulic oil is pumped into the sleeve until the pressure gauge connected to the sleeve reads 750 psi.

During the setup of the core holder, water is allowed to fill the water tank. When all line connections are made and confining pressure in the core holder is set, the pulse pump setting is verified and the pump is initiated. The pump is allowed to run until a steady flow of water exits the return line of the setup. This indicates that all of the air trapped in the lines and the core holder headspace has been flushed out of the system. Upon reaching the steady flow rate, the flow from the return line is collected in a graduated cylinder, timed over the course of one minute with a stopwatch. This is done to verify that the pump setting results in the correct pump output when no upstream back pressure is yet applied.

The backpressures on either side of the core holder are then applied. Firstly, the downstream regulator is set to 1,000 psi. This value is chosen because it needs to be higher than the vapor pressure of carbon dioxide at room temperature, which is produced as a byproduct of the reaction between calcium carbonate and hydrochloric acid. The downstream backpressure regulator is set by opening the flow of gas from the nitrogen tank connected to it until this pressure is reached. The upstream back pressure regulator is also set in this way, but in a stepwise manner of 250 psi increments until 1,000 psi is reached. Between each increment, confining pressure is added in 250 psi increments to the core holder through the hydraulic pump. This is done to ensure that the confining pressure around the core is always at least 750 psi higher than the upstream back pressure. This effectively prevents fluid from preferentially travelling along the side of the core and instead forces it to travel through the rock pores. Once the upstream backpressure reaches 1,000 psi, the pressure differential across the core is equalized. In order to induce an

interstitial velocity through the core, pressure is added to the upstream in order to increase the pressure differential.

The pressure differential relates to the interstitial velocity through Darcy's Law. The LabVIEW program used for this experiment records the interstitial velocity by way of a weight scale and calculates the flow rate of the effluent downstream of the core on the assumption that the density of the effluent is approximately the same as that of water. From this flow rate the interstitial velocity is obtained, and should match the value calculated through Darcy's Law based on the pressure differential induced across the core.

The acid solution is prepared in the acid tank, whose line to the pump is shut off while water is pumped through the system. An iOS timestamp application (Emerald) is used to record the moment when the line to the pump is switched from water to acid. It is important to note that the travel time of the acid from the pump to the nozzle is dependent on the flow rate of the acid. The inlet line consists of 3 segments:

Segment 1: Length = 18 in  ID = 1.0 in

$$V_1 = \frac{\pi}{4} D^2 L = \frac{\pi}{4} (1.0\ in)^2 (18.0\ in) = (14.158\ in^3) \left(16.3871 \frac{mL}{in^3}\right) = 232\ mL \quad (27)$$

Segment 2: Length = 14 in  ID = 0.402 in

$$V_1 = \frac{\pi}{4} D^2 L = \frac{\pi}{4} (0.402\ in)^2 (14.0\ in) = (1.7795\ in^3) \left(16.3871 \frac{mL}{in^3}\right) = 29\ mL \quad (28)$$

Segment 3: Length = 152 in  ID = 0.152 in

$$V_1 = \frac{\pi}{4} D^2 L = \frac{\pi}{4} (0.152\ in)^2 (152.0\ in) = (2.7622\ in^3) \left(16.3871 \frac{mL}{in^3}\right) = 46\ mL \quad (29)$$

Total: $232\ mL + 29\ mL + 46\ mL = 307\ mL$

The time required for the acid to displace the water volume in the inlet line is thus dependent on the injection flow rate from the pump:

$$t_{displace} = \frac{V_{total}}{q_{pump}} \tag{30}$$

This displacement time must be subtracted from the measured time between acid start and acid shutoff in order to determine the time spent only jetting acid from the nozzle.

Throughout each experiment, LabVIEW was used to monitor the change in interstitial velocity through the core and pressure differential. As mentioned in the experimental apparatus, two methods of control of the interstitial velocity were used: PID control and intermittent manual control. PID control is described in section 2.2 of the Experimental Setup. Both methods maintained a constant average effluent flow rate throughout the experiment.

Jetting time in each experiment was different. For the initial 16" cores and all of the 8" cores, jetting was allowed to continue until breakthrough, which causes a significant jump in effluent flow as the wormhole reaches the end of the core. Although this is a logic stop for an experiment, the lag in response time between the weight scale and control valve of the effluent means that the moment that breakthrough occurs is difficult to catch. In a large number of the 16" core experiments, jetting was allowed to continue just before breakthrough.

When the jetting time is stopped, the line leading to the pump is switched from the acid tank to the water tank. The upstream back pressure is immediately lowered in a reverse stage-wise manner as before the start of the experiment, in concert with lowering the confining pressure in the Viton sleeve. Water is allowed to circulate through the system

until all of the acid has been flushed from the lines. The removal of acid is confirmed through a pH strip giving a neutral reading at the flow of the return line. The confining pressure is lowered down to 750 psi and the pump is shut off. The lines to the core holder are subsequently disassembled and the core is removed from the core holder. The weight of the acidized core is then recorded.

### *3.2.4 Modifications to Procedure*

In this study, 22 of the experiments done of 4" by 16" Indiana limestone cores were performed with the above procedure. For 6 experiments performed on Indiana limestone cores with dimensions 4" by 8", the adjusted pump procedure was used. For those latter experiments, the return line was not allowed to recycle acid back into the acid tank, therefore allowing the acid tank concentration to remain the same throughout the experiment.

High temperature experiments were performed with a heat exchanger water bath installed between the pump and the core holder. The water bath was turned on before the start of the experiment to allow the fluid pumped through it to come out at the desire 180°F temperature.

## 3.3 Post-Experimental Processing

After the completion of each experiment, the cores were scanned in a Toshiba Aquilon TSX-101A/RG Computer Tomography (CT) machine, shown in Figure 3.6.

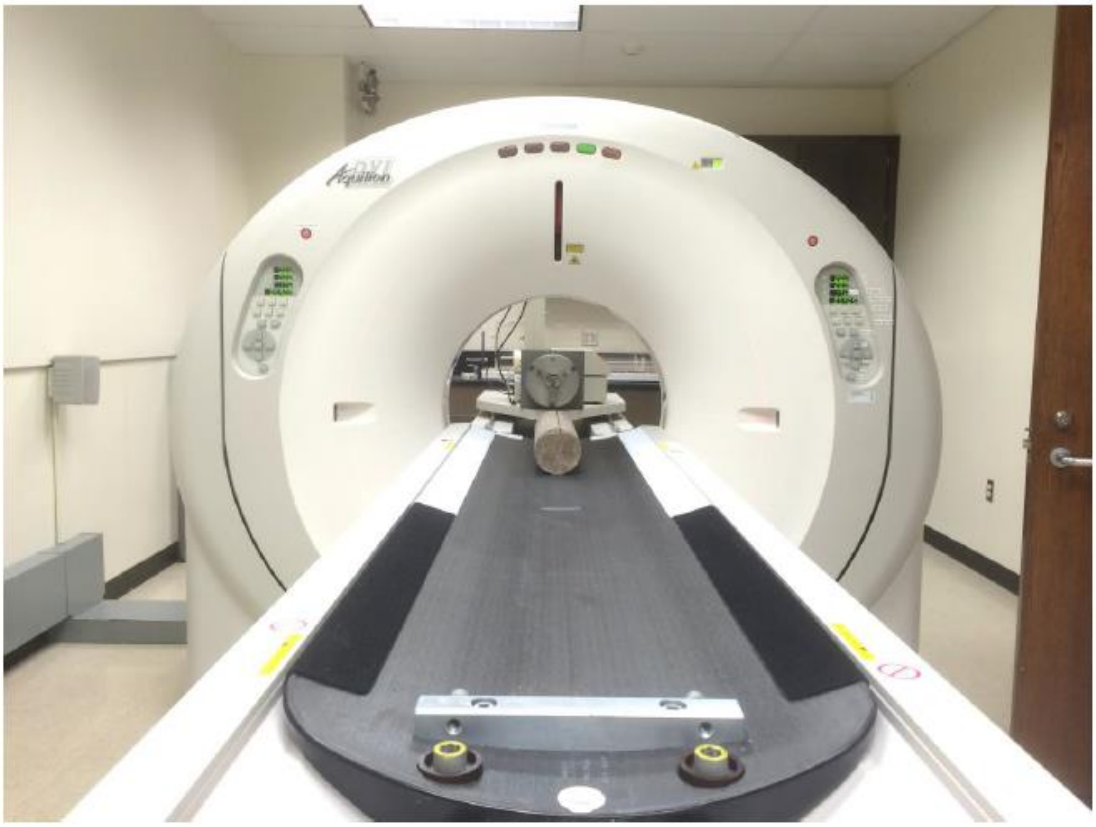

**Figure 3.6 - Toshiba Aquilon CT Scanner**

A vertical line was drawn on the side of each core to ensure that it was aligned in the scanner. The scanned images were obtained in the form of a DICOM file in sets of cross sectional images of the core. Figure 3.7 shows one of these images. A full description of the CT image rendering process has been described by Belostrino (2016). For this study, the images were rendered by way of an open source program called Horos and image retrieving software is an extension called ImageJ.

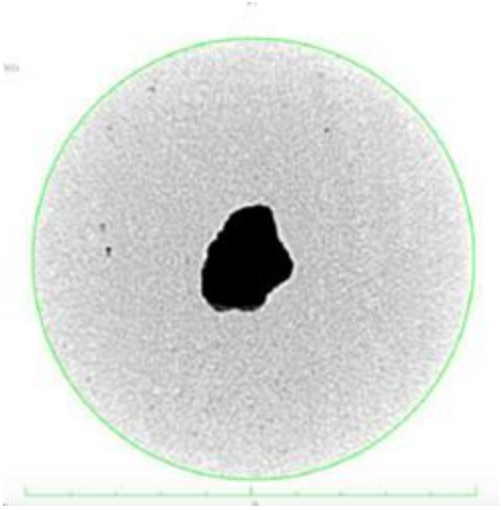

**Figure 3.7 - Acid Jetting DICOM Image in Horos with ROI (region of interest)**

The full workflow for the image processing is the following:

Uploading Documents

1. Open ImageJ → Plugins → Tudor DICOM → DICOM Manager
2. Click folder icon (first on the left) in DICOM Manager
3. In new window, click DICOM QUERY → click search icon (top right corner)
4. Look for "Patient Name" along with "Patient ID" to identify correct core
5. Click on desired core → click on "Study ID" → click on "Retrieve to Local"
6. Find file saved in Home (H:) → DICOMSTORE → "Patient Name"

Transfering Documents

1. Download files to desired storage device (USB etc.)
2. Transfer files from storage device to desired location on Mac computer

3D Volume Rendering in Horos

1. Open Horos → Click "Import" → Find desire file and click "open"

2. Option box will ask “Copy files or copy links” → Click “Copy Links” to save memory space
3. For 3D volume rendering, open the 3rd image set and start from the 1st image of the set
4. Click “Oval Tool” → Manipulate oval to fit core image → Click “Propagate Selected ROI”
5. Under “Propagate current selected ROI(s) to:” select up to image number → Enter 100 or other necessary value to fit oval on core
6. Under “Copy Method” select “Create Aliases” → Click Ok
7. For the last set of propagated ROIs, the ROI will need to be propagated to the total number of images minus 1 image number
8. Click “ROI” → Click “Save All ROIs of this Series”
9. Save ROI in desired location as “Core ID ROI”
10. Click “ROI” → Click “Set pixels values too” → Under “Apply to:” select “ROIs with same name as the selected ROI
11. Under “Set pixels that are:” select “Outside ROI”
12. Select “To this new value:” and enter “3024” → Click Ok
13. Click “3D Viewer” → Click “3D Volume Rendering”
14. Change level of detail to “Fine” on the toolbar
15. Select “16 bit” and histogram will appear at bottom of the screen
16. Move points within histogram to reveal dissolution structure → Double click on all points and change all points to 100% Whiteness

17. Once the desired level of clarity is achieved, Click “16 bit”, and the histogram will disappear
18. Click “Magnifying Glass” icon to change zoom level to 0.125%
19. Click “File” → Click “Export” → Click “Export to Movie”
20. Set “Number of frames:” to 360 → Under “Rotation:” select “360 degrees” and “Horizontal” → Under “Quality:” select “Best rendering” → Under “Size:” select “Current” → Click Ok
21. Adjust “Frame rate:” to desired level (Default value = 20)
22. Under “Format:” select “H264 Movie”
23. Name file as “Core ID HiRes” → Click Save
24. Click “Measurement Tool” and measure length of wormholes (if not broken through) → Make sure line is vertically straight for accurate measurement
25. Click “File” → Click “Export” → Click “Export to JPEG”
26. Name file “Core ID Wormhole Length (xx.xx cm)” → Click Save
27. Repeat process for cavity depth → Name file “Core ID Cavity Depth (xx.xx cm)” → Click save
28. Note: Cavity Depth can be calculated using images numbers ((image # at start of cavity – image # at end of cavity) * image thickness (1 mm or 0.333 mm))

<u>Cavity Volume Calculation</u>

1. In Horos, open 4th image set of desired file
2. Record the first image number representing “cavity volume”

3. Right click on 4th image set → click “Open Sub-Selection” → Under “From:” enter the first image number representing “cavity volume” → Under “To:” enter “500” → Click Ok
4. Click “ROI” → click “Grow Region (2D/3D Segmentation)” → Under “Lower Threshold” enter “-3000” → Under “Upper Threshold” enter “100” → Under “ROI Name” enter “Core ID Cavity Volume”
5. Click within area of cavity on first image representing “cavity volume” → Click “Compute”
6. Find image number which represents termination of the “cavity volume” and “wormholing” begins (based on minimum area or other criteria established)
7. The “actual” image number where this termination occurs will be the current image plus the image number of the “first” image minus 1
8. Close window → Right click on 4th image set → click “Open Sub-Selection” → Under “From:” enter the first image number representing “cavity volume” → Under “To:” enter “actual image number representing termination of cavity” → Click Ok
9. Click “ROI” → Click “ROI Volume” → Click “Compute Volume”
10. Press “Command+Shift+4” → Press Spacebar → Click in the “ROI Volume” window to take screenshot → File will be saved on Desktop, moved file to appropriate folder
11. Click “File” → Click “Export” → Click “Export to JPEG”
12. Name file “Core ID Cavity Volume (xx.xxxx cc)” → click “Save

# 4. RESULTS & DISCUSSION

The results of 28 acid jetting experiments are discussed in this study, performed on Indiana limestone cores. The experiments are grouped by sets according to the variable investigated in the group, such as the interstitial velocity, jetting velocity, acid temperature and acid concentration. The experiments were conducted to examine the relationship between the cavity and wormhole formation in jetting. The experimental conditions and core properties are listed in Appendix 1.

It is important to note that only for 6 of the Indiana limestone experiments the jetting velocity was accurately kept constant throughout the entire range of tested interstitial velocities. For the experiments performed earlier, the pumping rate was kept constant across the range of jetting velocities in the assumption that it would result in a constant jetting velocity, but due to the upstream pressure being different at each interstitial velocity setting, the output of the pump was caused to subsequently change, resulting in a differing jetting velocity than initially anticipated. Therefore, these 6 experiments were used as the baseline trend for the acid jetting phenomenon, with all other experiments analyzed in reference to this data.

## 4.1 Quantifying the Outcome of Acid Jetting

In matrix acidizing, the volume of injected acid flows only through the core, and is thus equivalent to the volume of effluent flowing out of the rock. The volume of acid needed to be injected in order for a wormhole to form to the end of core divided by the porous volume of the rock is referred to as the pore volume to break through (PVbt), and is used

as a metric of efficiency in an acidizing treatment. The lower the value of the pore volume to breakthrough value is, the less acid is needed to fully penetrate through the core, and the smallest such volume is thus the most efficient. Although acid jetting also creates wormholes like in matrix acidizing, there is a fundamental difference in the flow path of the injected acid between the two scenarios.

In acid jetting, acid is injected into the core holder by way of a narrow nozzle, producing a high velocity stream. Based on the set pressure differential applied across the core, there is a specific matrix flow rate of liquid that can travel through the rock at its inherent permeability according to Darcy's Law. However, the injection rate needed to achieve the high velocity in the jet through the nozzle is always higher than the matrix flow rate. As a result, not all of the injected acid can travel through the rock and must therefore be evacuated from the headspace of the core holder. Figure 4.1 displays the difference in the flow paths between matrix acidizing and acid jetting. It is also important to note that this flow path difference occurs mainly as a result of the experimental setup. In the field, the injected acid flows out of the limited entry liner orifices and impinges on the rock face, and the acid that does not enter the formation at the impingement point travels elsewhere in the annulus.

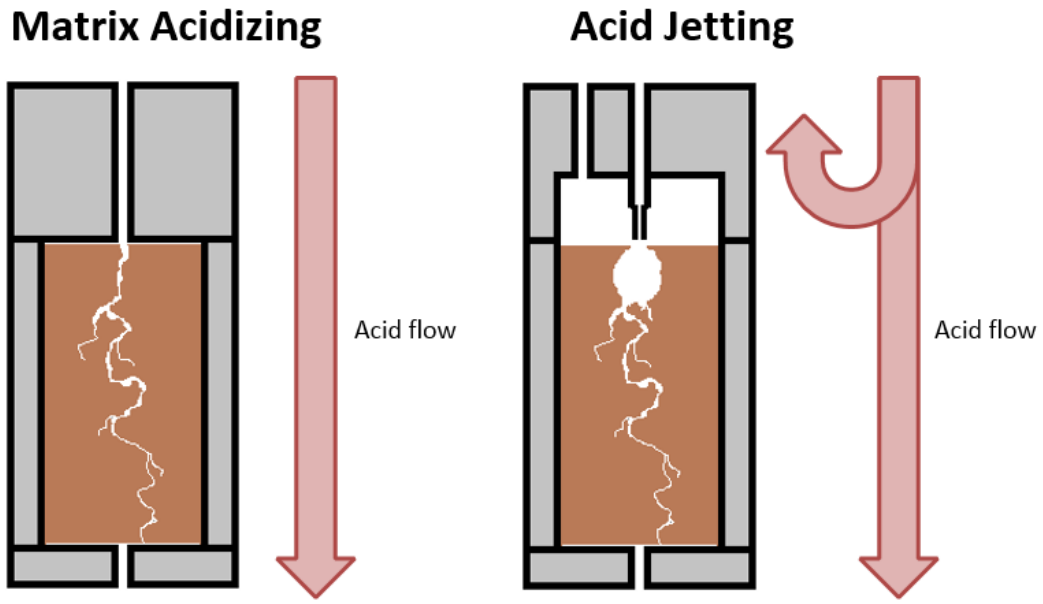


**Figure 4.1 - Flow path comparison between matrix acidizing and acid jetting core flood experiments**

This poses a question of how efficiency is defined in acid jetting in in lab-scale experiments. A calculation of pore volume to breakthrough can be attempted in two ways: determination of the volume of acid needed to dissolve the volume of rock occupied by the cavity and wormhole, or by the determination of the value by only accounting for the flow through the core. In matrix acidizing, these two calculations would yield the same result, since all of the injected acid travels through the rock. In acid jetting however, those two values are different, and neither one gives an objectively comparable value to that of matrix acidizing.

### *4.1.1 Challenges of Calculating PVbt Based on Effluent Flow*

This method calculates the volumes of acid required to propagate a wormhole given the effluent flow rate, thereby interstitial velocity through the rock. The relationship between effluent flow rate ($q_{effluent}$) and interstitial velocity ($v_i$) is:

$$v_i = \frac{q_{effluent}}{A\phi} \tag{31}$$

Where $\phi$ is the porosity of the rock and $A$ is the cross-sectional area of the flow. The relationship between pore volume to breakthrough based on interstitial velocity as calculated for matrix acidizing is:

$$PV_{bt} = \frac{v_i t_{jet}}{L_{wh}} \tag{32}$$

Where $t_{jet}$ is the jetting velocity and $L_{wh}$ is the wormhole length from the surface. The main issue with using this relationship with regards to acid jetting is that the $PV_{bt}$ value obtained ignores any of the acid volume spent on the creation of the cavity, assuming that the entire length of $L_{wh}$ from the top of the core to the end is occupied solely by the wormhole. Although the wormhole in most cases extends much farther beyond the cavity, and based on results obtained by Belostrino (2016) the wormhole does form at the same time as the cavity from the original surface of the core, this relationship presents an artificially lower volume of acid needed to break through the core.

### *4.1.2 Challenges of Using PVbt Based on Dissolved Rock Volume*

This method calculates the volumes of acid required to dissolve the volume of rock equivalent to the volume of the cavity and the wormhole in the core. This based on the

dissolving power of the acid at the tested concentration ($\chi_{15}$). The volume of calcium carbonate dissolved ($V_{CaCO_3}$) is obtained from CT images of the dissolution structure after acidizing.

$$V_{HCl} = \frac{V_{CaCO_3}}{\chi_{15}} \quad where \quad \chi_{15} = 0.0829 \frac{cm^3\ CaCO_3}{cm^3 15\%\ HCl} \tag{33}$$

$$V_{pore} = \frac{\pi}{4} D_{core}^2 L_{core} \phi \tag{34}$$

$$PV_{bt} = \frac{V_{HCl}}{V_{pore}} \tag{35}$$

It is clear from this calculation method that in every case, acid jetting dissolves a significantly higher volume of rock than matrix acidizing would at an equivalent effluent flow rate, and is thus always less efficient in terms of acid use than matrix acidizing. However, based on the results collected in this study, it is evident that although a higher volume of acid is needed to break through the core in acid jetting, this does not mean that the dissolution front (i.e. wormhole) travels at a slower rate in acid jetting than it would in matrix acidizing at a given interstitial velocity.

### *4.1.3 Wormhole Growth Rate as a Performance Metric*

Wormhole growth rate in any acidizing experiment is calculated as the length of wormhole through the core over the acidizing time.

$$v_{wh} = \frac{L_{wh}}{t_{jet}} \tag{36}$$

This value is calculated in the same way for both matrix acidizing and acid jetting experiments, and is not dependent on the flow path of the acid. It is therefore a more

objective metric by which the outcome of acid jetting can be analyzed and directly compared to a case where a jet is not present. It is important to note that wormhole growth rate is not proportional to wormhole efficiency and this study does not imply that a faster wormhole growth rate is equivalent to a more optimal use of acid.

### 4.2 Effect of Interstitial Velocity on Wormhole Growth Rate

Three sets of experiments were performed to examine the relationship of acid jetting dissolution as a relationship of interstitial velocity, which can be found in Appendix 1. The experiments for Set 1 were performed with a continuously controlled interstitial velocity throughout the jetting time by PID control of the effluent flow rate. The interstitial velocity in Set 2 was controlled only when its value increased to more than 25% above the set point value. These experiments were performed with the intention of determining whether continuous PID control and movement of the needle valve induced a deleterious choking effect on the effluent line. The experiments in Set 1 and 2 were done before the determination of the pump output relationship with the upstream core pressure, and as a result have a true jetting velocity significantly below the assumed 150 ft/s value, and also have a gradient with respect to upstream core holder pressure (and ultimately interstitial velocity). The experiments in Set 3 were run with the intention of having a consistent jetting velocity across all interstitial velocities. To achieve this, pump rates were adjusted and tested before the beginning of jetting in each experiment. Figure 4.2a, 4.2b and 4.2c display the CT images of the cores from Sets 1, 2, and 3 respectively.

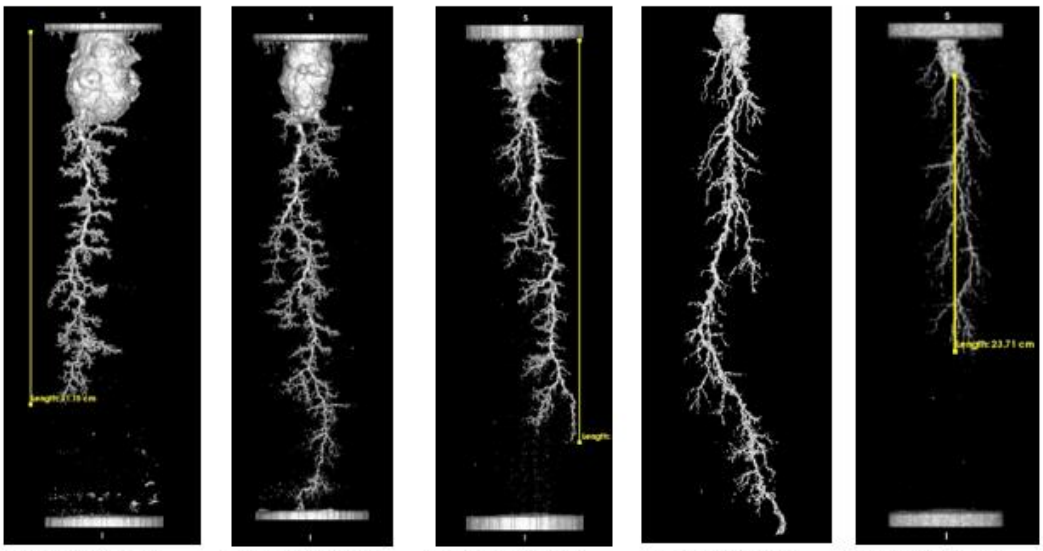

$v_i$ = 0.20 cm/min
$v_{wh}$ = 0.52 cm/min

$v_i$ = 0.30 cm/min
$v_{wh}$ = 1.08 cm/min

$v_i$ = 0.51 cm/min
$v_{wh}$ = 1.90 cm/min

$v_i$ = 1.00 cm/min
$v_{wh}$ = 2.31 cm/min

$v_i$ = 1.51 cm/min
$v_{wh}$ = 1.46 cm/min

**Figure 4.2a - CT scan images of PID control acid jetting experiments (Set 1)**

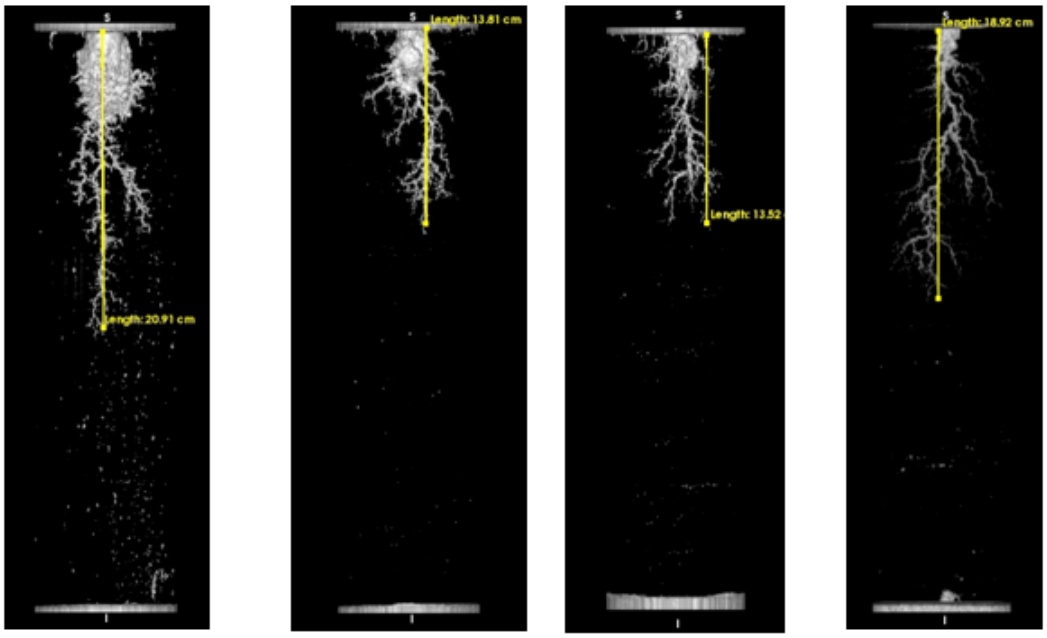


$v_i$ = 0.21 cm/min
$v_{wh}$ = 1.09 cm/min

$v_i$ = 0.39 cm/min
$v_{wh}$ = 1.60 cm/min

$v_i$ = 0.74 cm/min
$v_{wh}$ = 2.76 cm/min

$v_i$ = 1.52 cm/min
$v_{wh}$ = 1.03 cm/min

**Figure 4.2b - CT scan images of intermittent interstitial velocity control acid jetting experiments (Set 2)**

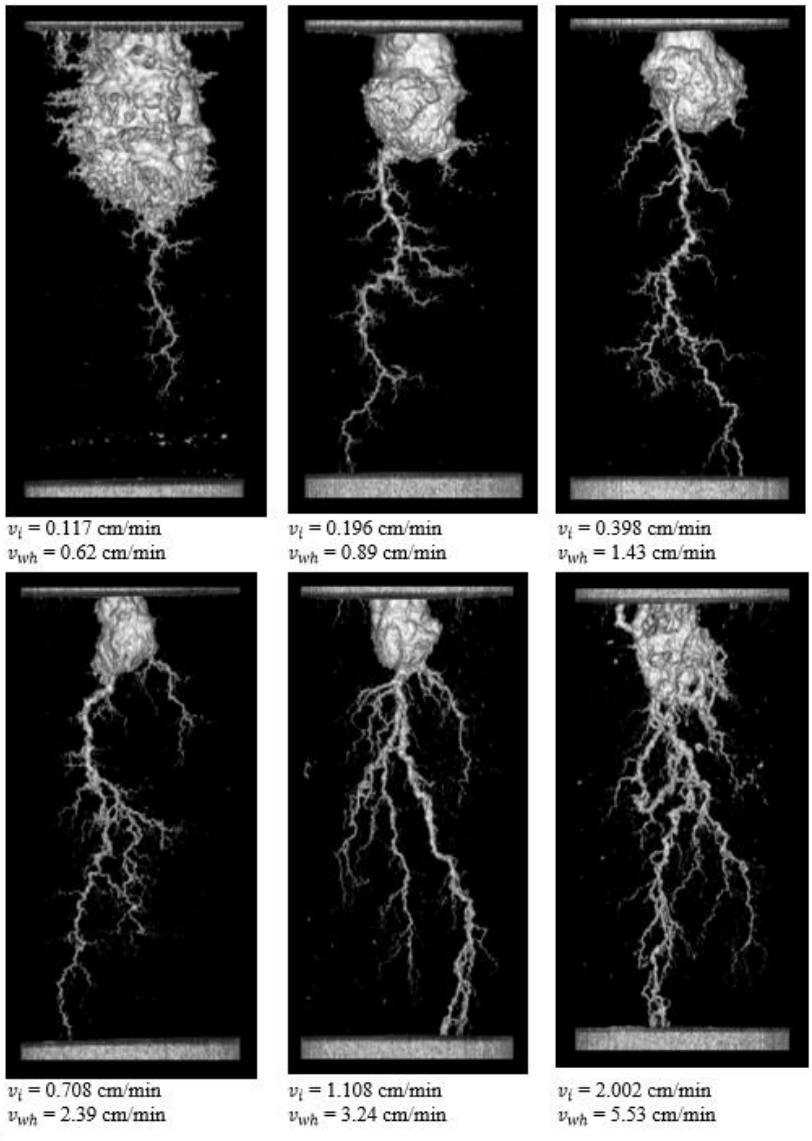


**Figure 4.2c - CT scan images of constant jetting velocity acid jetting experiments (Set 3)**

It can be seen that as the interstitial velocity varies from 0.1 cm/min to 2.0 cm/min, the wormholes produced are similar to those produced in a flow loss regime. This is different than the transition from compact dissolution regime to a fluid loss regime observed in matrix acidizing core floods. The wormhole growth rate for experiments in Set 1, 2 and 3

were calculated and Figure 4.3 displays the resulting wormhole growth rate for all three sets of experiments as a function of interstitial velocity.

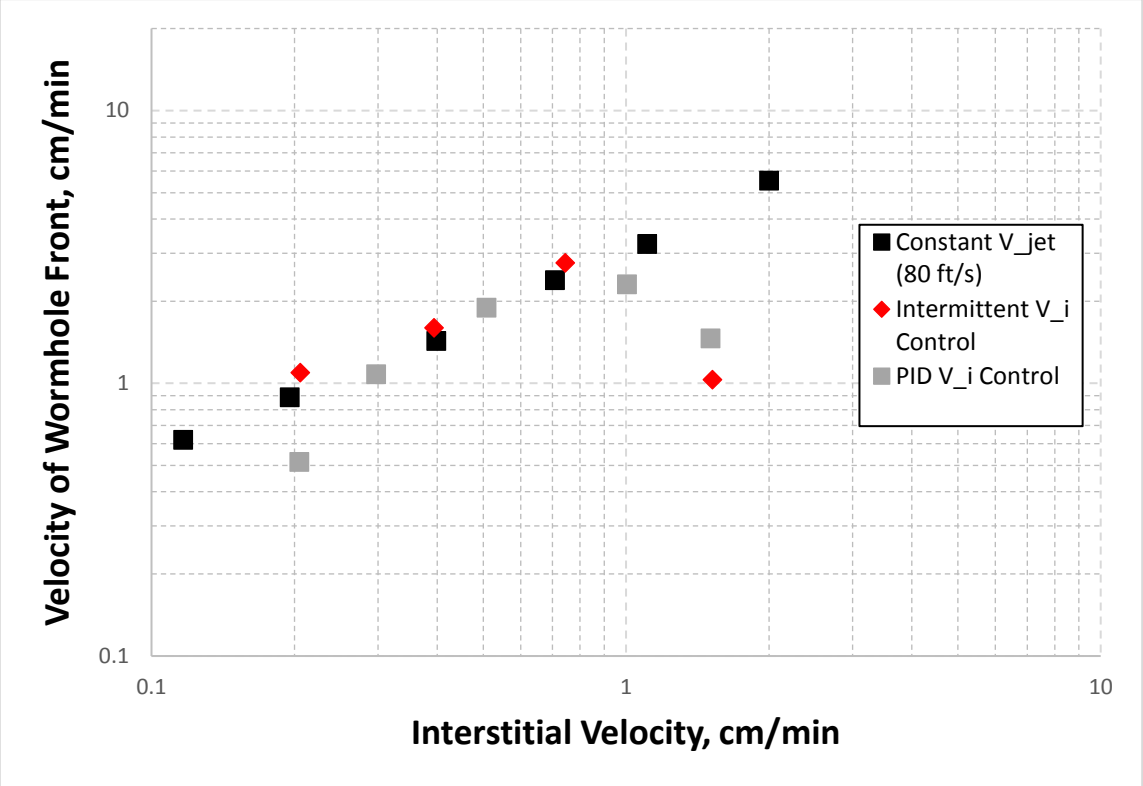


**Figure 4.3 - Wormhole growth rate as a function of interstitial velocity in acid jetting experiments**

It can be observed that for the experiments performed at a constant jetting velocity, there is a linear relationship between interstitial velocity and wormhole growth rate on a log-log plot. Interestingly, the experiments performed at jetting rates that were variable have similar wormhole growth rate values, with the exception of very high interstitial velocities. It can be inferred that jetting velocities in this range has a limited effect on wormhole growth rate.

The discrepancy in wormhole growth rates at high interstitial velocities is due to an experimental artefact. High interstitial velocities require higher upstream core holder pressure. If the upstream pressure nears the pump threshold of 1900 psi, the pump rate decreases to the point of creating almost no jetting velocity. This also means that the time necessary to displace the fresh water in the core holder headspace is longer, and for a majority of the jetting time the concentration of acid flowing into the rock is exceedingly low, thereby causing a dramatic drop in wormhole growth rate. When the jetting velocity is corrected to a constant value in Set 3, it was observed that this experimental artefact disappears and the trend in wormhole growth rate is proportional to the increase in interstitial velocity.

### 4.3 Effect of Jetting Time on Cavity Growth Rate

The experiments in Set 3 were conducted at a constant pump flow rate of 385 mL/min, producing a jetting velocity of 82 ft/s. The flow rate of the effluent from the core is dependent on the interstitial velocity experienced through the rock, and is in the range of 1.12 mL/min to 25.77 mL/min for the tested points. Since the effluent flow rate is only a small fraction of the flow rate from the pump, the majority of the injected acid does not flow through the core, and instead travels through the return line and varies by at most 6% (382 mL/min at vi = 0.1 cm/min to 360 mL/min at vi = 2.0 cm/min)

In the work of Ndonhong et al. (2017), it is discussed that the dominant mechanism in the formation of the cavity in acid jetting is surface dissolution caused by acid not penetrating the rock. If the flow rate of the return line across all tested interstitial velocities

varies at most by 6%, it can be inferred that interstitial velocity has a very weak influence on the formation of the cavity. This conclusion may seem counterintuitive upon examination of the cavity size across the tested cores in Set 3, since higher interstitial velocity cores have smaller cavities than cores ran at lower interstitial velocities. The difference in size however, is accounted for by the jetting time. Cores ran at higher interstitial velocities have smaller jetting times than those ran at lower interstitial velocities. Figure 4.4 displays the growth rate of the cavity of a core plotted against the jetting time of that core on a log-log plot. It can be observed that there is an exponentially decaying rate of growth of the cavity as jetting time increases. Based on this relationship, it can be inferred that the cavity will continue to slow in growth asymptotically and will eventually approach a size at which growth is negligible.

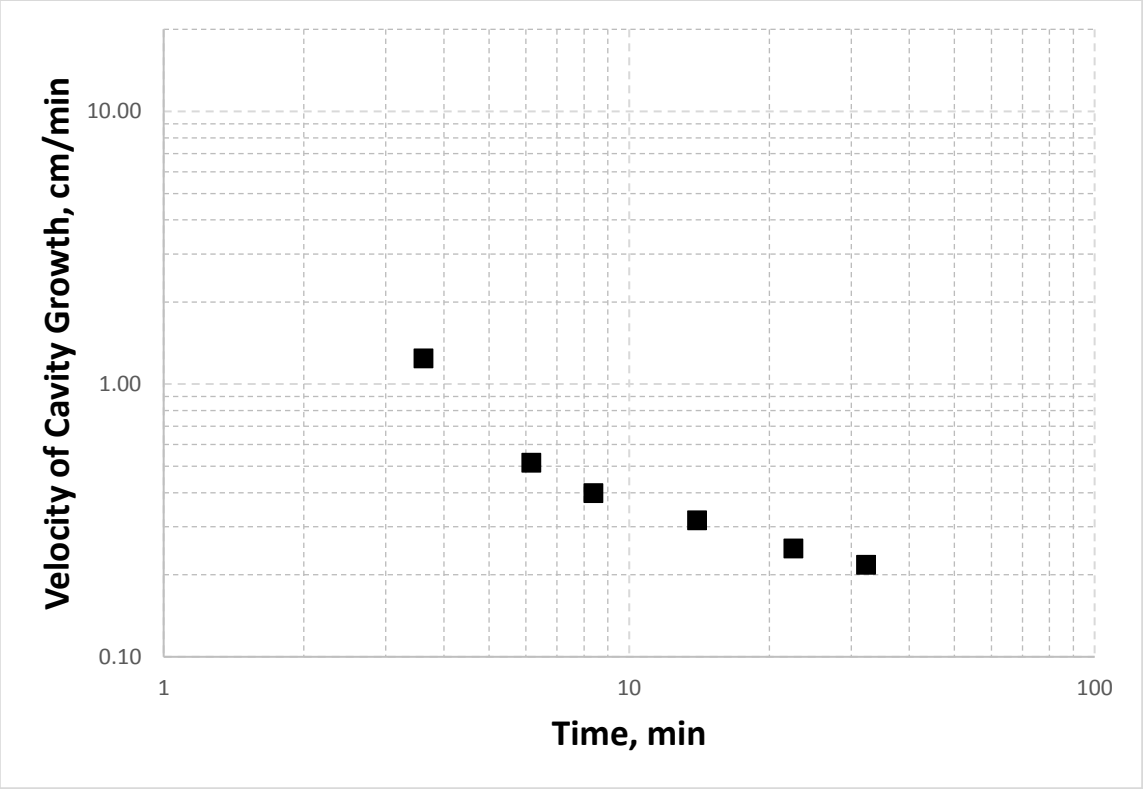


**Figure 4.4 - Cavity growth rate as a function of time for constant jetting velocity acid jetting experiments (Set 3)**

It is important to note that as the cavity increases in depth with jetting time, the standoff distance between the tip of the nozzle and the surface of the rock on which the jet impinges grows longer.

### 4.4 Comparison of Jetting and Non-Jetting Wormhole Growth Rate

In order to isolate the effect of a jet on wormhole growth rate in this experimental apparatus, three experiments were conducted in which the injected acid entering the headspace of the core holder was mechanically dispersed. The dispersion eliminates the high velocity stream impinging on the surface of the rock, causing only wormholes and

no cavity to form. The data for these experiments can be found in Set 4 of Appendix 1. Figure 4.5 displays the CT images of these non-jetting experiments.

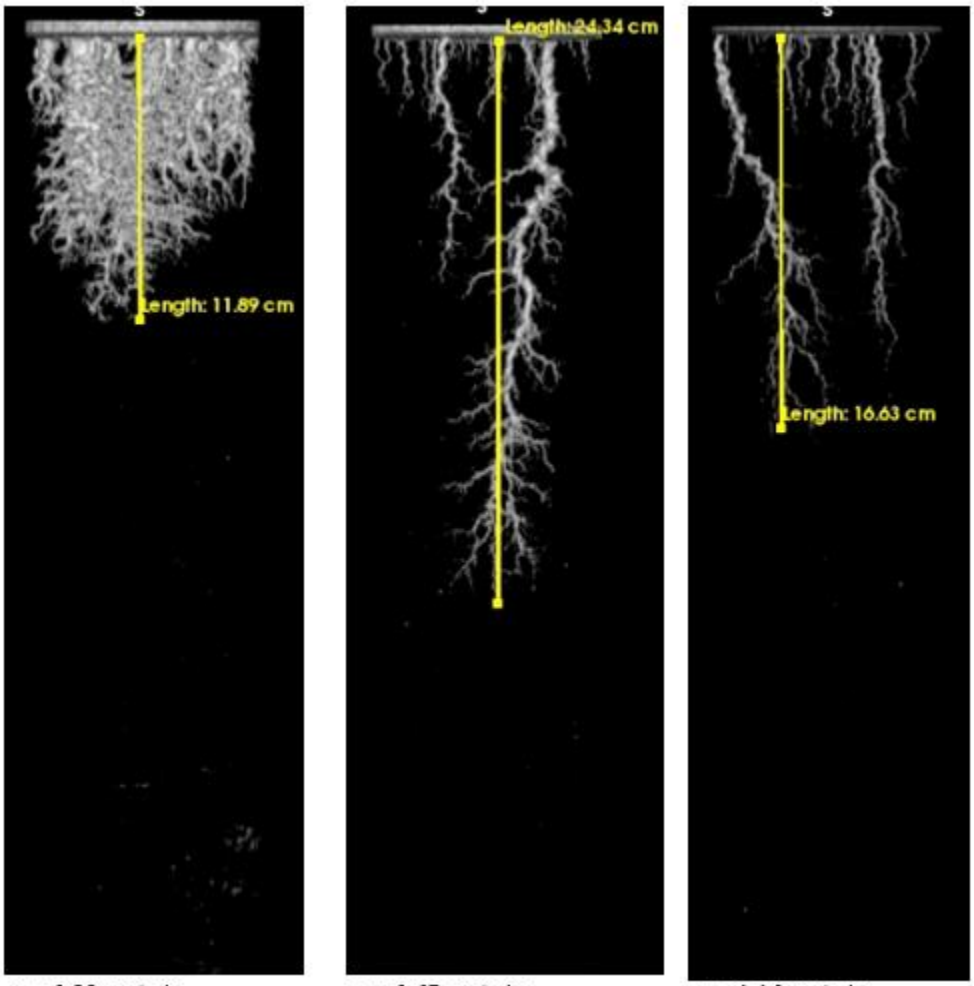


**Figure 4.5 - CT scan images of non-jetting experiments (Set 4)**

Figure 4.6 displays the relative trend wormhole growth rates of the jetting and non-jetting experiments with respect to interstitial velocity.

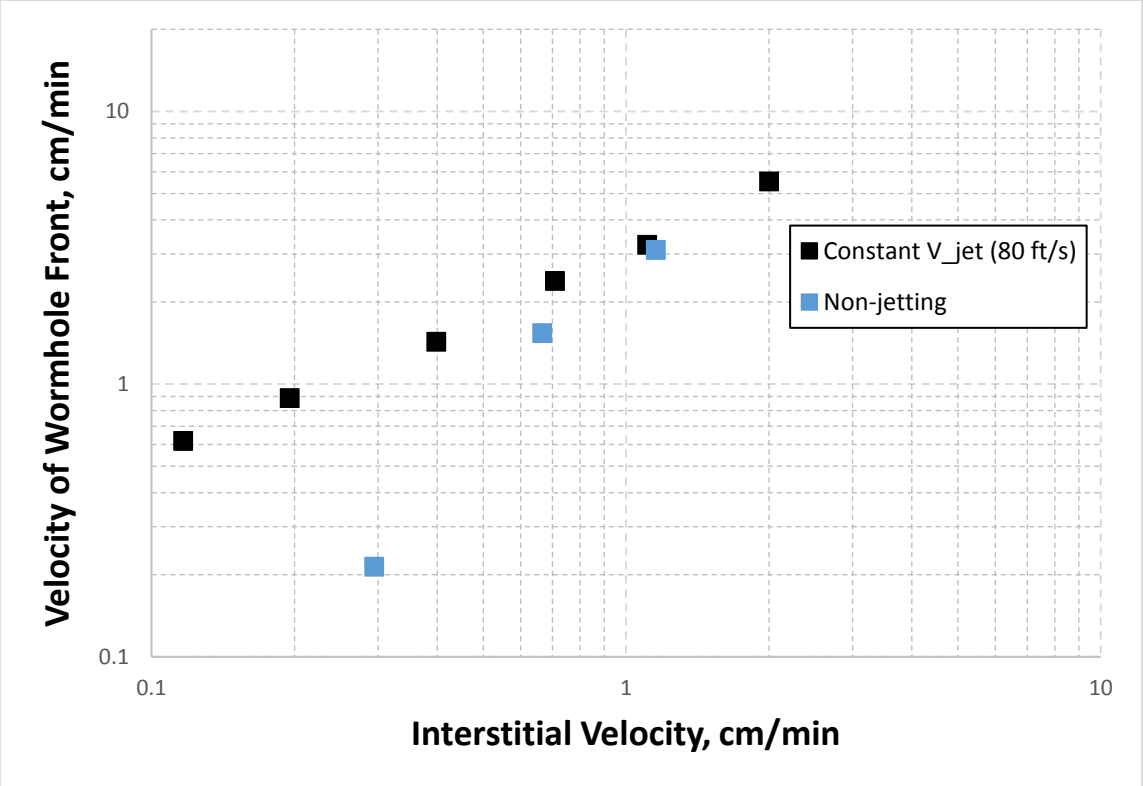


**Figure 4.6 - Wormhole growth rates for constant jetting velocity and non-jetting experiments as a function of interstitial velocity**

It can be observed that at lower interstitial velocities, jetting produces a significantly faster growing wormhole than a non-jetting case at an equivalent flow rate through the rock. As interstitial velocity increases, the wormhole growth rate trends of jetting and non-jetting approach one another, eventually overlapping. This convergence may be due to the impingement pressure caused by the jetting becomes progressively smaller relative to the upstream pressure required to induce higher interstitial velocities, thus muting the effect of jetting in raising the wormhole growth rate through the core. Further experimentation is required to verify whether the two trends continue their convergence at interstitial velocities of 2.0 cm/min and above.

If this acid jetting data were to be fit with a Buijse-Glasbergen wormhole propagation model, the resulting fit corresponds to an absence of compact dissolution. The fit is essentially linearly proportional to interstitial velocity.

It would appear that the presence of the jet eliminates or significantly reduces compact dissolution during the jetting time period recorded in the experiments of this study. This is evident from the appearance of the wormholes observed in jetting at low interstitial velocities being similar in appearance to those otherwise formed at higher interstitial velocities in matrix acidizing. This observation however neglects the significant surface dissolution caused by the formation of the cavity.

### 4.5 Effect of Jetting Velocity on Wormhole Growth Rate

Three acid jetting experiments were conducted at a constant interstitial velocity of 0.3 cm/min and variable jetting velocities and can be found as Set 5 in Appendix 1. Figure 4.7 displays CT images of these experiments with increasing jetting velocity.

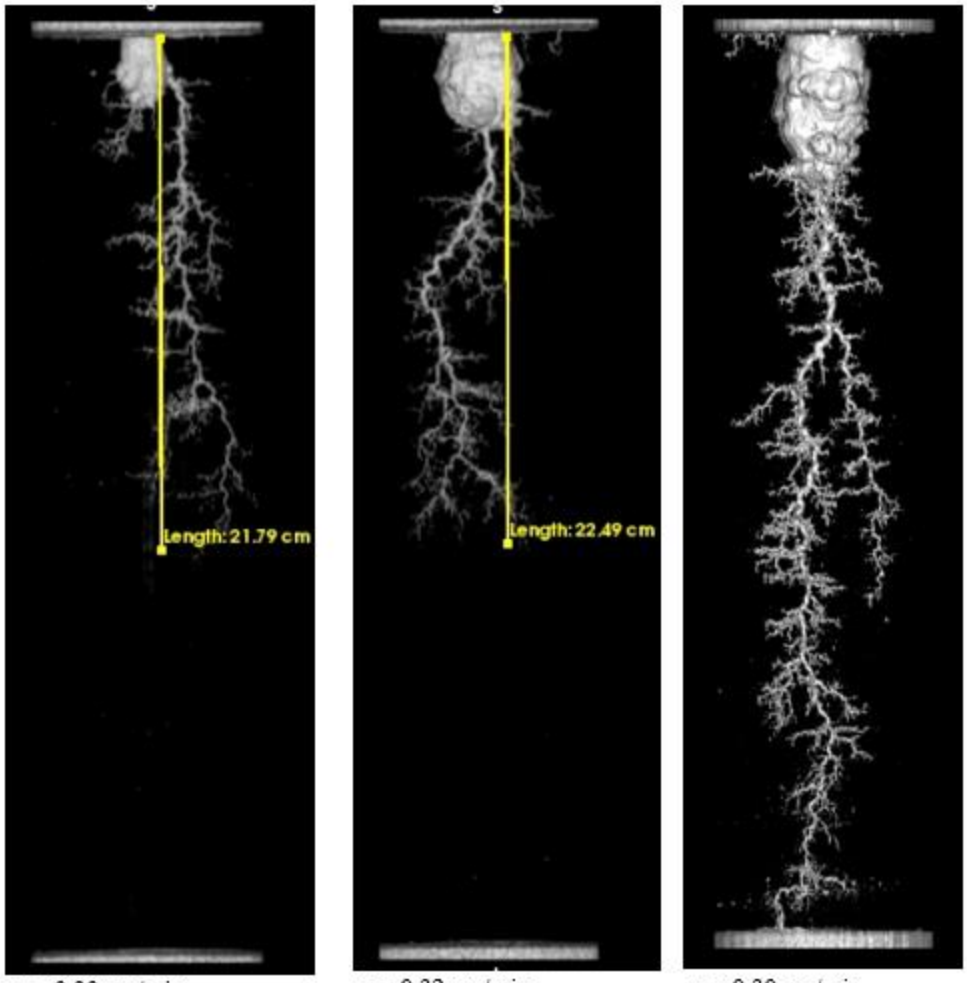


**Figure 4.7 - CT scan images of acid jetting experiments at lowered jetting velocities (Set 5)**

Figure 4.8 displays the wormhole growth rates of these experiments with respect to jetting velocity, as well as an interpolated wormhole growth rate value from the experiments performed in Set 3 with a constant jetting velocity of 80 ft/s.

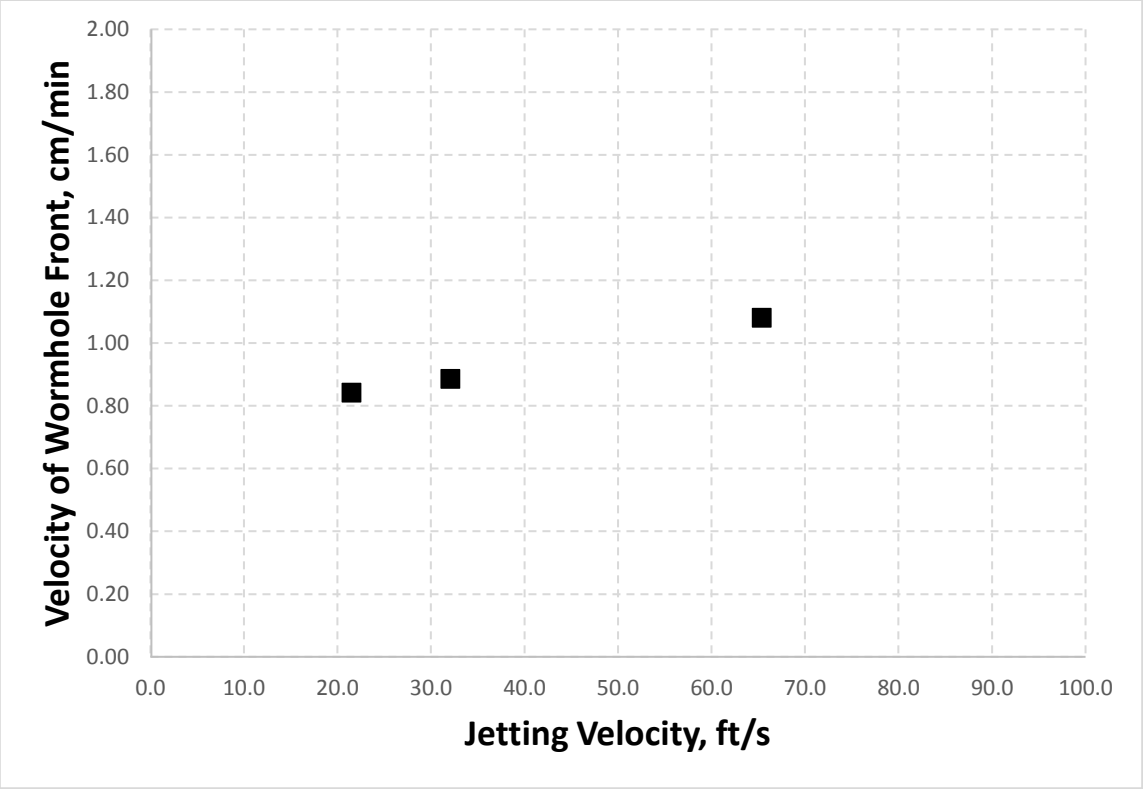


**Figure 4.8 - Wormhole growth rate for acid jetting experiments at a constant interstitial velocity (0.3 cm/min) as a function of jetting velocity**

There is a proportional relationship between increasing jetting velocity and increasing wormhole velocity in the range of 20 ft/s to 82 ft/s of jetting velocity. The wormhole velocity increases by approximately 36% in this range, meaning that intervals of 10 ft/s in jetting velocity produce only a 6% difference in wormhole growth rate. The low sensitivity of wormhole growth rate to jetting velocity can be used to explain the similarity in wormhole growth rate between experiments in Set 3 and Sets 1 and 2. Further experimentation is required to verify whether the same trend continues for jetting velocities above 82 ft/s and what the trend is for jetting below 20 ft/s.

### 4.6 Effect of Jetting Velocity on Cavity Growth Rate

A similar plot to Figure 4.8 can be made for the trend of cavity growth rate in the same experiments, displayed in Figure 4.9.

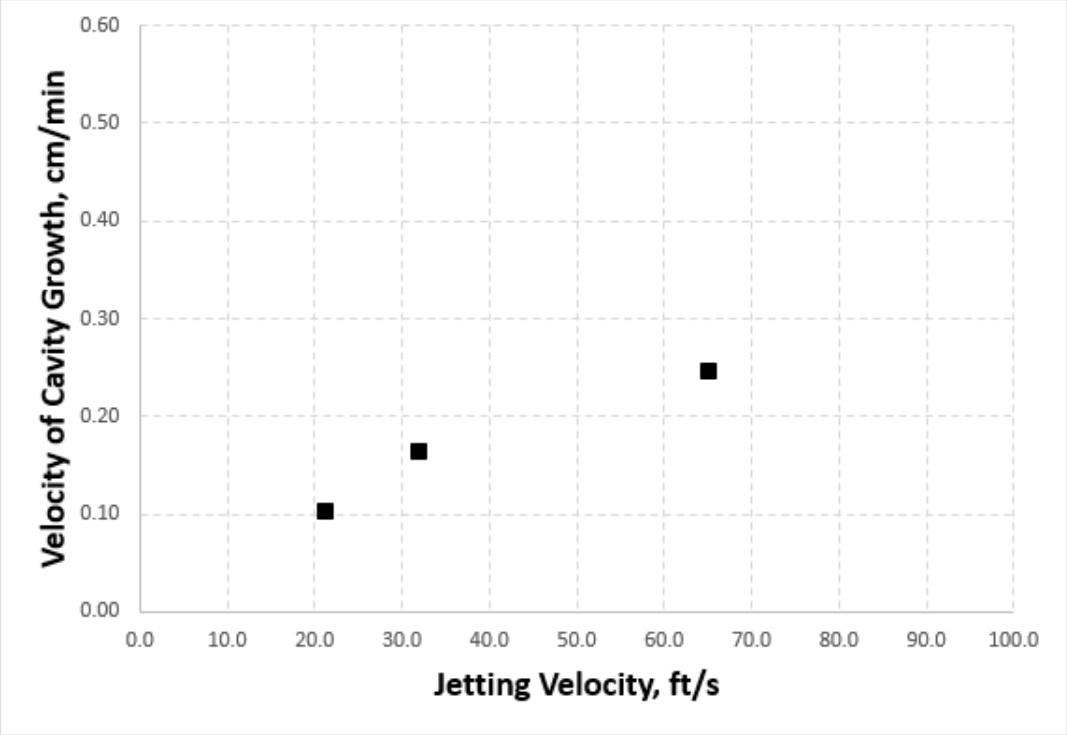


**Figure 4.9 - Cavity growth rate for acid jetting experiments at a constant interstitial velocity (0.3 cm/min) as a function of jetting velocity**

A logarithmic trend is observed in this case, with cavity growth rate commencing after jetting velocity is applied, and subsequently tapering off with progressively higher jetting velocities. Cavity growth may be more sensitive to jetting velocity than wormhole propagation. This also agrees with the findings of Ndonhong (2014) and the non-jetting experiments conducted in Set 4, which produced no cavity in the absence of a jet.

### 4.7 Relationship of Cavity Growth Rate to Wormhole Growth Rate

The cavity and wormholes grow simultaneously during the acid jetting process, and both are influenced by a different set of parameters. The cavity grows as a result of the jetting velocity and time, but is negligibly influenced by interstitial velocity or the wormholes that propagate beyond the cavity. Wormhole growth rate on the other hand, is primarily influenced by interstitial velocity and less strongly by the velocity of the jet. In matrix acidizing, the constant flow through the core also means that the growth rate of the wormholes is constant throughout the acidizing time. In acid jetting however, wormhole growth rate changes as the depth of the cavity increases with time.

Further experimentation is required to better understand the relationship between the increase in cavity depth that leads to an increase in nozzle to rock standoff, and the corresponding change in wormhole growth rate.

### 4.8 Effect of Temperature on Cavity Growth Rate

Three acid jetting experiments were conducted at an elevated temperature of 180°F to give an approximation of the dissolution change at downhole temperatures. The data for these experiments can be found as Set 6 in Appendix 1. Figure 4.10 displays the CT scan images of these experiments. Negligible wormholing was observed in these experiments, despite the formation of a large cavity in each case. This finding is

consistent with previous studies done on high temperature acid jetting by Ndonhong (2017).

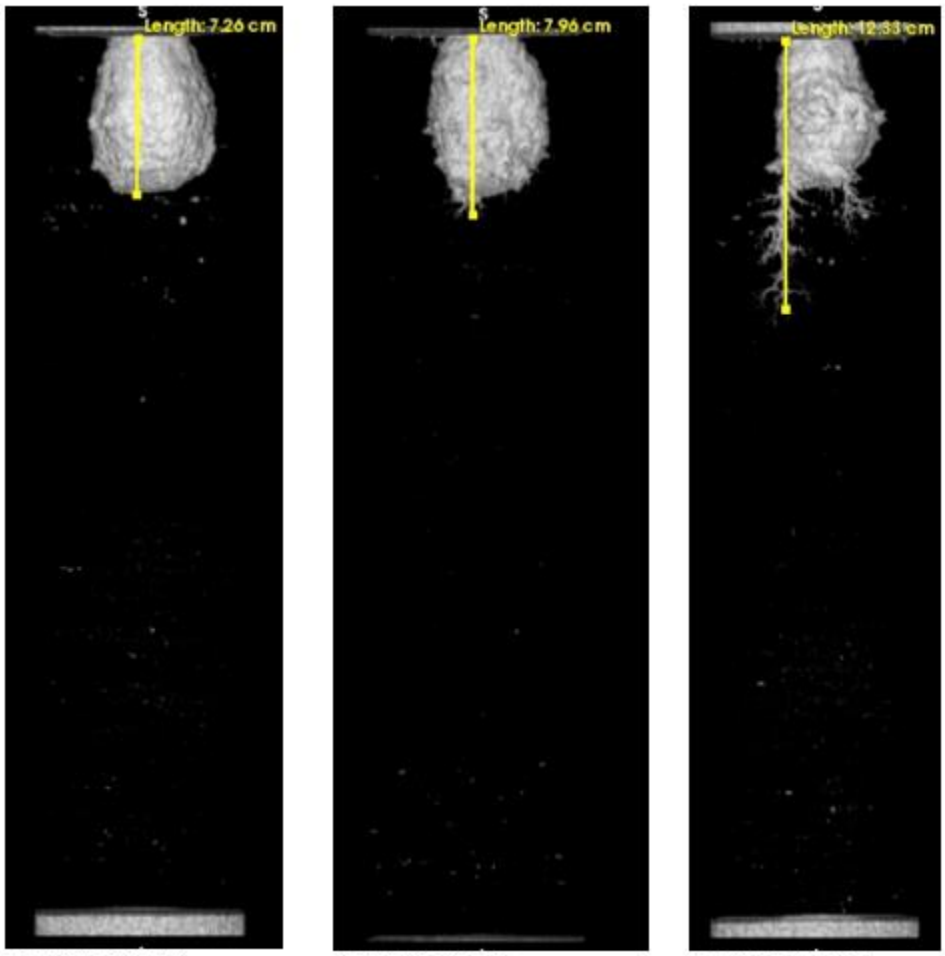


**Figure 4.10 - CT scan images of acid jetting experiments performed at elevated temperature (180°F, Set 6)**

These experiments were performed prior to the determination of the change in pump output with upstream backpressure, so the jetting velocity on these experiments is similar but not consistent. The lack of wormholing indicates that compact dissolution

prevails in at higher temperatures in this setup, meaning that it is possible that higher interstitial velocities will be needed to generate wormhole growth rates observed at room temperature. Since cavity growth rate is negligibly influenced by interstitial velocity, the effect of interstitial velocity on high temperature acid jetting requires further study with longer experiments. The current experimental setup is limited by the 4" diameter of the core holder and future experiments involving high temperature would be better performed on wider samples.

### 4.9 Effect of Acid Concentration on Cavity and Wormhole Growth Rates

Three experiments were conducted at an elevated concentration of HCl to better understand the effect of acid concentration on acid jetting dissolution. The experiments were conducted with a 28% weight concentration rather than the baseline of 15%, and the experimental data can be found as Set 7 in Appendix 1. Figure 4.11 shows the CT scan images of the cores with increasing interstitial velocity.

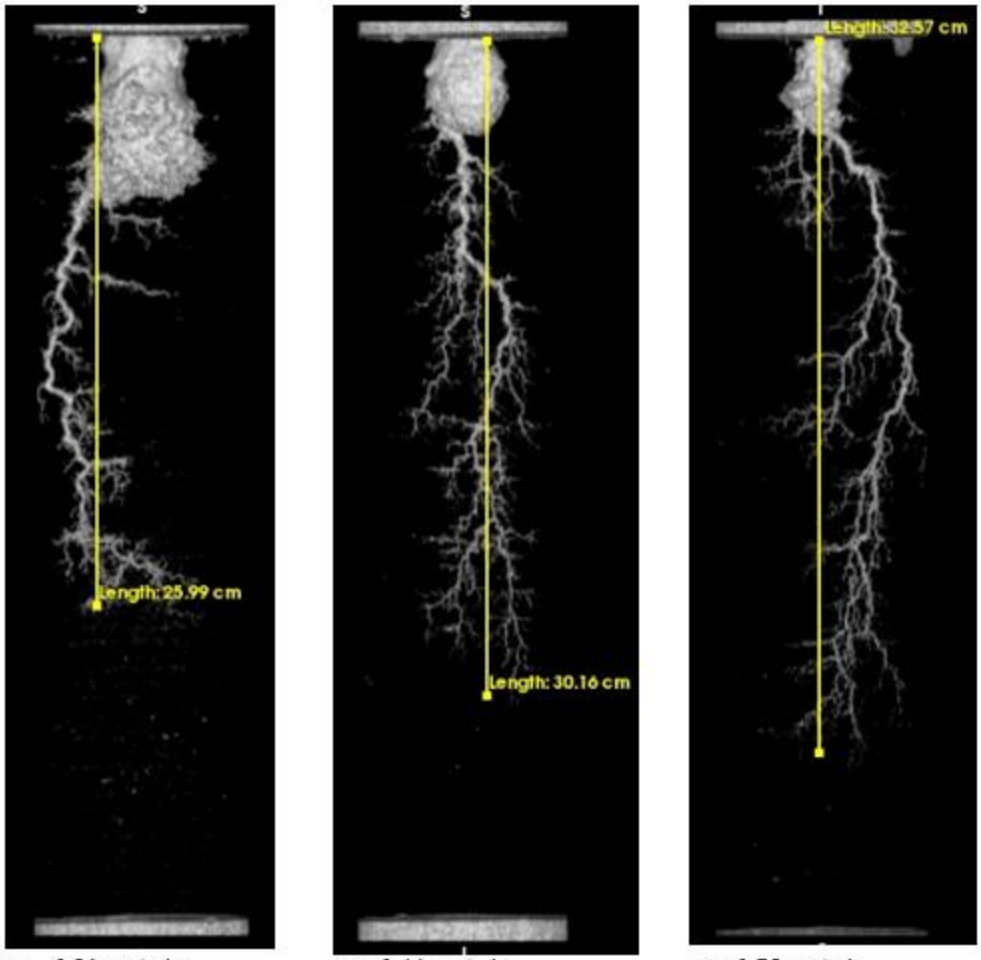


$v_i$ = 0.21 cm/min
$v_{jet}$ = 53 ft/s
$v_{wh}$ = 0.84 cm/min

$v_i$ = 0.44 cm/min
$v_{jet}$ = 62 ft/s
$v_{wh}$ = 2.18 cm/min

$v_i$ = 0.75 cm/min
$v_{jet}$ = 72 ft/s
$v_{wh}$ = 3.48 cm/min

**Figure 4.11 - CT scan images of 28% acid concentration jetting experiments (Set 7)**

The structure of the cavity and wormholes is very similar to that which is obtained with the baseline concentration. Figure 4.12 displays the wormhole growth rate of these experiment versus those obtained with 15% concentration in Set 2.

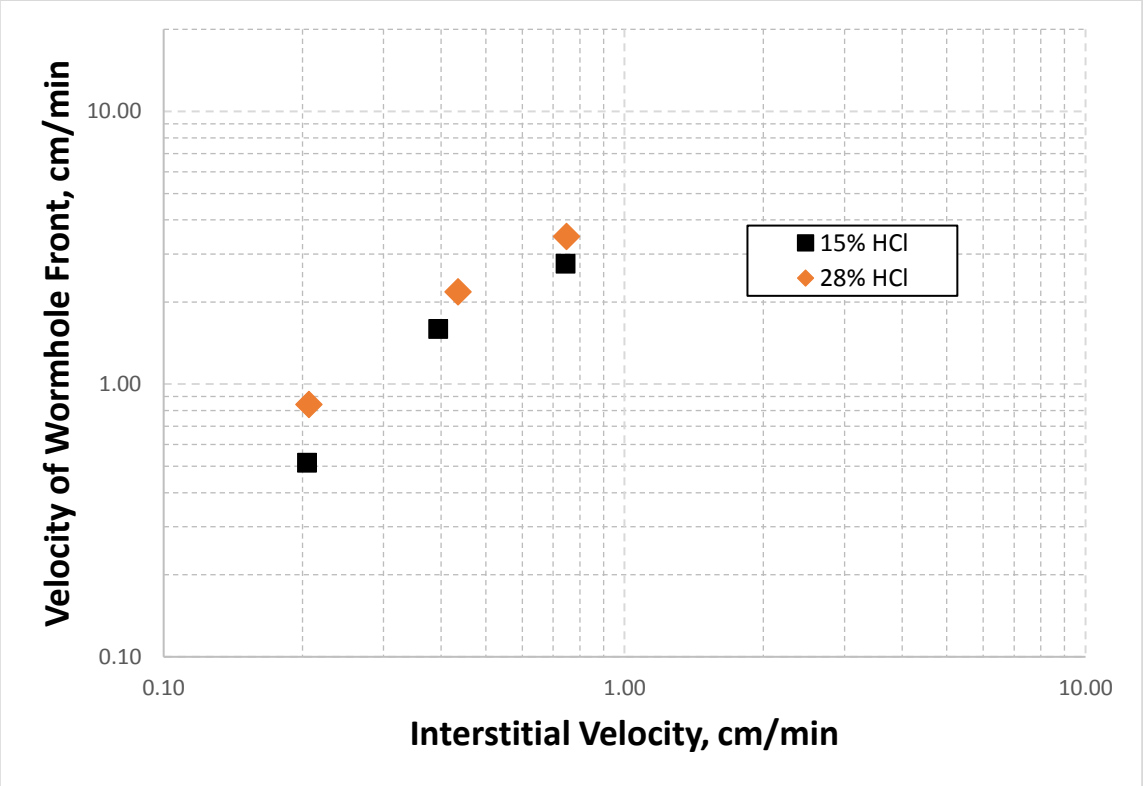


**Figure 4.12 - Wormhole growth rate comparison between 15% and 28% acid concentration jetting experiments as a function of interstitial velocity**

It is important to note that as with the high temperature experiments in Set 6, these experiments were performed prior to the determination of the change in pump output with upstream backpressure, so the jetting velocity on these experiments is similar but not consistent. For this reason this set was compared with the intermittent control experiments from Set 2 rather than the adjusted experiments with constant jetting velocity from Set 3. It can be seen that there is a slight overall increase in wormhole growth at all interstitial velocities for experiments with a 28% acid concentration, despite having twice the amount of hydrochloric acid per volume available to react.

# 5. CONCLUSIONS & FUTURE WORK

Overall, this study has fulfilled its aim of providing an objective means of comparison of acid jetting to non-jetting core floods, as well as characterizing the effect of transport conditions such as temperature, jetting velocity, and acid concentration on the outcome of the dissolution in acid jetting.

Operationally, this study demonstrated a new procedure of recording and controlling the effluent flow from the core holder, allowing for a constant interstitial velocity to be maintained throughout the experiment. This was achieved through PID control and subsequent Ziegler-Nichols tuning. This control technique was contrasted with intermittent manual control of the interstitial velocity and has not shown any significant difference in acid jetting outcome between the two techniques. Furthermore, a previously unreported decreasing behavior of the acid injection pump output has been identified, and its relationship with increasing upstream backpressure has been characterized. This allows for the pump to be set and tested prior to each experiment to ensure a constant flow acid rate through the system at various induced pressure differentials across the core holder.

The results of the acid jetting experiments have shown that acid jetting has a high rate of wormhole growth than a non-jetting test, with the difference being larger at lower interstitial velocities. The wormhole growth rates for acid jetting and non-jetting appear to converge at progressively higher interstitial velocities. It has also been found that cavity growth is negligibly influenced by interstitial velocity, with dominant variables instead being jetting velocity and jetting time. An exponentially decaying relationship has been observed between cavity growth rate as a function of jetting time, with the cavity

continuing to growth more slowly with time. The asymptote of growth rate does not approach zero within the experimental timeframe looked at in the scope of this study. The influence of jetting velocity on wormhole growth has been shown to be weakly proportional between velocities of 20 ft/s and 80 ft/s. Jetting velocity has been shown to have a much steeper relationship with cavity growth rate than with wormhole growth rate.

Higher temperature significantly increases compact dissolution in the experiments, to the point that only cavities and no wormholes are observed in the tests. Higher acid concentration has a weak but positive overall effect on wormhole growth rate on all tested interstitial velocities.

Future work is recommended to include new tests run with the appropriate pump verification procedure to ensure a constant jetting velocity when varying interstitial velocity. Further experimentation is required to better understand the effect of cavity depth increase and corresponding change in wormhole growth, as well as the relationship between jetting velocity and wormhole growth at very low jetting velocities (20 ft/s and lower). The trends described also need to be investigated and verified for longer jetting times than the experimental setup can permit (due to size limitations of how much the cavity and wormhole can grow). Furthermore, future experiments can be performed in a radial rock geometry in order to better correlate the findings of this study to the behavior of acid jetting downhole.

## REFERENCES


Beckham, R.E., Shuchart, C. E., and Buechler, S. R. 2015. Impact of Acid Jetting on Carbonate Stimulation. Paper IPTC 18360-MS presented at the International Petroleum Technology Conference. Doha, Qatar. 6-9 December.

Belostrino, E.P. 2016. Experimental Study of Multi-Stage Acid Jetting in Carbonate Rocks. MS Thesis. Texas A&M University. College Station, Texas.

Buijse, M.A. and Glasbergen, G. 2005. A Semiempirical Model to Calculate Wormhole Growth in Carbonate Acidizing. Paper SPE 96892 presented at the SPE Annual Technical Conference and Exhibition. Dallas, Texas. 9 October.

Fredd, C. N., & Fogler, H. S. (1999, September 1). Optimum Conditions for Wormhole Formation in Carbonate Porous Media: Influence of Transport and Reaction. Society of Petroleum Engineers. doi:10.2118/56995-PA

Furui, K., Fuh, G.-F., Abdelmalek, N. A., & Morita, N. (2010, December 1). A Comprehensive Modeling Analysis of Borehole Stability and Production-Liner Deformation for Inclined/Horizontal Wells Completed in a Highly Compacting Chalk Formation. Society of Petroleum Engineers. doi:10.2118/123651-PA

Glasbergen, G., & Buijse, M. A. (2006, January 1). Improved Acid Diversion Design using a Placement Simulator. Society of Petroleum Engineers. doi:10.2118/102412-MS

Grabski, E.R. 2012. Matrix Acidizing Core Flooding Apparatus: Equipment and Procedure Description. Master of Science. Texas A&M University. College Station, Texas.

Hansen, J. H. and Nederveen, N. 2002. Controlled Acid Jet (CAJ) Technique for Effective Single Operation Stimulation of 14,000 ft Long Reservoir Sections. Paper SPE-78318-MS presented at the European Petroleum Conference. Aberdeen, United Kingdom. 29–31 October.

Hoefner, M. L., & Fogler, H. S. (1989, February 1). Fluid-Velocity and Reaction-Rate Effects During Carbonate Acidizing: Application of Network Model. Society of Petroleum Engineers. doi:10.2118/15573-PA

Hung, K. M., Hill, A. D., & Sepehrnoori, K. (1989, January 1). A Mechanistic Model of Wormhole Growth in Carbonate Matrix Acidizing and Acid Fracturing. Society of Petroleum Engineers. doi:10.2118/16886-PA

Holland, C.C. 2014. Experimental High Velocity Acid Jetting in Limestone Carbonates. MS Thesis. Texas A&M University. College Station, Texas.

Jackson, Alfred , John Jorden, and Mohamed Abdulla Al Marzouqi. 2011. Completion and Stimulation Challenges and Solutions for Extended-Reach Multizone Horizontal Wells in Carbonate Formations. Proc., SPE Middle East Oil and Gas Show and Conference, Manama, Bahrain.

Jackson, Alfred, Badr Musabbeh Al Azizi, and Curtis Kofoed. 2012. Completion and Stimulation Methodology for Long Horizontal Wells in Lower Permeability Carbonate Reservoirs. Proc., Abu Dhabi International Petroleum Exhibition & Conference, Abu Dhabi, United Arab Emirates.

Johnson, A., Eslinger, D., and Larsen, H. 1998. An Abrasive Jetting Scale Removal System. Paper SPE-46026-MS Presented at the SPE/ICoTA Coiled Tubing Roundtable. Houston, Texas. 15–16 March.

Jorden, J. D., Jackson, A. M., Keller, S. R., Shuchart, C. E., Alvarez, J. O., & Quigley, M. S. (2011, January 1). Pre-perforated Liner Design and Coiled-Tubing Acidizing of Maximum-Reservoir-Contact (MRC) Wells Offshore Abu Dhabi. Society of Petroleum Engineers. doi:10.2118/140244-MS

Ndonhong, V. 2014. Observations from Experimental Acid Jetting on Limestone Carbonates. MS Thesis. Texas A&M University. College Station, Texas.

Ndonhong, V., Belostrino, E., Zhu, D., Hill, A. D., Beckham, R. E., & Shuchart, C. E. 2016. The Impact of Rock Properties on Acid Jetting in Carbonate Rocks: An Experimental Study. Paper SPE 180113-MS presented at thw SPE Europec featured at 78th EAGE Conference and Exhibition. Vienna, Austria. 30 May-2 June.

Ritchie, B., Abbasy, I., Pitts, M., White, B. and Rushdun Jaafar, M. 2008. Challenges in Completing Long Horizontal Wells Selectively. Paper SPE 116541 presented at SPE Asia Pacific Oil and Gas Conference and Exhibition, Perth, Australia. 10/20/2008

Sau, R., A. Goodrow, M. Rockwell, C. Mayer, C. E. Shuchart, and M. A. Grubert, 2014. An Integrated Software Technology Based on Research and Field Application for Completion, Stimulation and Fluid Placement Design in Complex Wells. Paper IPTC-17870-MS presented at the International Petroleum Technology Conference. Kuala Lumpur, Malaysia. 10-12 December.

Sau, R., C. E. Shuchart, and M. Grubert, 2014. Advanced Completion and Stimulation Design Model for Maximum Reservoir Contact Wells. Paper SPE-171800-MS

presented at the Abu Dhabi International Petroleum Exhibition and Conference. Abu Dhabi, UAE. 10-13 November.

Schwalbert, M. P., Zhu, D., & Hill, A. D. (2017, June 12). Extension of an Empirical Wormhole Model for Carbonate Matrix Acidizing Through Two-Scale Continuum 3D Simulations. Society of Petroleum Engineers. doi:10.2118/185788-MS

Shuchart, C. E. 2014. Completion and Stimulation of Maximum Reservoir Contact and Complex Wells. Presentation at the SPE Stimulation Applied Technology Workshop, Abu Dhabi, UAE. 24-25 February.

Surjaatmadja, J., Abass, H., and Brumley, J. 1994. Elimination of Near-Wellbore Tortuosities by Means of Hydrajetting. Paper SPE 28761 presented at the Asia Pacific Oil and Gas Conference. Melbourne, Australia. 7-10 November.

## APPENDIX 1

| Set | Description | Porosity (%) | Permeability (mD | Pump Setting (%) | Pump Flow rate (mL/min) | Jetting velocity (ft/s) | Interstitial Velocity (cm/min) | Jetting time (min) | Cavity depth (in) | Wormhole Length (cm) | Wormhole growth rate (cm/min) | Cavity growth rate (cm/min) |
|---|---|---|---|---|---|---|---|---|---|---|---|---|
| 1 | PID control of $v_i$ | 14.1 | 2.11 | 68.5 | 319.5 | 68.1 | 0.20 | 61.6 | 8.10 | 31.15 | 0.52 | 0.13 |
| | | 14.4 | 2.35 | 68.5 | 102.3 | 21.8 | 1.51 | 16.2 | 3.11 | 23.71 | 1.46 | 0.16 |
| | | 14.8 | 2.52 | 68.5 | 164.9 | 35.1 | 1.00 | 17.6 | 5.20 | 40.64 | 2.31 | 0.27 |
| | | 15.1 | 2.48 | 68.5 | 275.3 | 58.7 | 0.51 | 18.1 | 6.07 | 34.31 | 1.90 | 0.32 |
| | | 15.3 | 2.17 | 68.5 | 306.6 | 65.4 | 0.30 | 37.6 | 9.43 | 40.64 | 1.08 | 0.24 |
| 2 | Intermittent control of $v_i$ | 13.8 | 1.58 | 68.5 | 312.1 | 66.5 | 0.21 | 19.1 | 6.44 | 20.91 | 1.09 | 0.32 |
| | | 12.8 | 2.36 | 68.5 | 256.9 | 54.8 | 0.74 | 4.9 | 2.67 | 13.51 | 2.76 | 0.44 |
| | | 12.8 | 2.38 | 68.5 | 304.8 | 65.0 | 0.39 | 8.7 | 4.70 | 13.81 | 1.60 | 0.49 |
| | | 13.8 | 3.28 | 68.5 | 175.9 | 37.5 | 1.52 | 18.3 | 2.55 | 18.92 | 1.03 | 0.13 |
| 3 | Constant $v_{jet}$ | 14.9 | 4.02 | 83.0 | 385.0 | 80.0 | 0.398 | 14.00 | 4.43 | 19.77 | 1.428 | 0.32 |
| | | 14.2 | 2.53 | 81.4 | 385.0 | 80.0 | 0.196 | 22.53 | 5.63 | 19.77 | 0.888 | 0.25 |
| | | 13.8 | 2.00 | 79.6 | 385.0 | 80.0 | 0.117 | 32.28 | 7.02 | 19.77 | 0.620 | 0.22 |
| | | 15.9 | 5.72 | 85.2 | 385.0 | 80.0 | 0.708 | 8.38 | 3.34 | 19.77 | 2.387 | 0.40 |
| | | 15.9 | 9.91 | 85.2 | 385.0 | 80.0 | 2.002 | 3.62 | 4.50 | 19.77 | 5.530 | 1.24 |
| | | 15.4 | 8.89 | 92.0 | 385.0 | 80.0 | 1.108 | 6.17 | 3.18 | 19.77 | 3.243 | 0.52 |
| 4 | Non-jetting | 15.2 | 2.26 | 68.5 | 304.8 | 0.0 | 0.29 | 56.6 | 0.00 | 11.90 | 0.21 | 0.00 |
| | | 15.3 | 3.3 | 68.5 | 253.2 | 0.0 | 0.67 | 17.0 | 0.00 | 24.30 | 1.54 | 0.00 |
| | | 15.1 | 2.48 | 68.5 | 179.6 | 0.0 | 1.16 | 7.0 | 0.00 | 16.63 | 3.11 | 0.00 |
| 5 | Lowered $v_{jet}$ | 13.7 | 2.24 | 68.5 | 301.1 | 1.4 | 0.31 | 65.9 | 8.23 | 29.57 | 0.46 | 0.12 |
| | | 12.7 | 3.07 | 40.0 | 100.9 | 21.5 | 0.36 | 28.9 | 2.90 | 21.79 | 0.84 | 0.10 |
| | | 13.5 | 3.06 | 20.0 | 150.4 | 32.1 | 0.32 | 27.5 | 4.44 | 22.58 | 0.89 | 0.16 |
| 6 | High temperature (180°F) | 14.8 | 3.27 | 68.5 | 304.8 | 65.0 | 0.39 | 13.6 | 6.97 | 7.96 | 0.63 | 0.51 |
| | | 14.3 | 3.58 | 68.5 | 288.2 | 61.4 | 0.74 | 13.9 | 6.81 | 12.33 | 0.96 | 0.49 |
| | | 13.5 | 3.19 | 68.5 | 334.2 | 71.2 | 0.21 | 14.7 | 7.26 | 0.00 | 0.00 | 0.49 |
| 7 | High acid concentration (28% w HCl) | 14.0 | 2.89 | 68.5 | 247.7 | 52.8 | 0.75 | 10.6 | 4.41 | 32.57 | 3.48 | 0.42 |
| | | 13.4 | 2.71 | 68.5 | 291.9 | 62.2 | 0.44 | 14.9 | 4.30 | 30.16 | 2.18 | 0.29 |
| | | 13.8 | 3.67 | 68.5 | 337.9 | 72.0 | 0.21 | 31.8 | 7.70 | 25.99 | 0.84 | 0.24 |